$7

QEX

May/June 2018

www.arrl.org

A Forum for Communications Experimenters

Issue No. 308

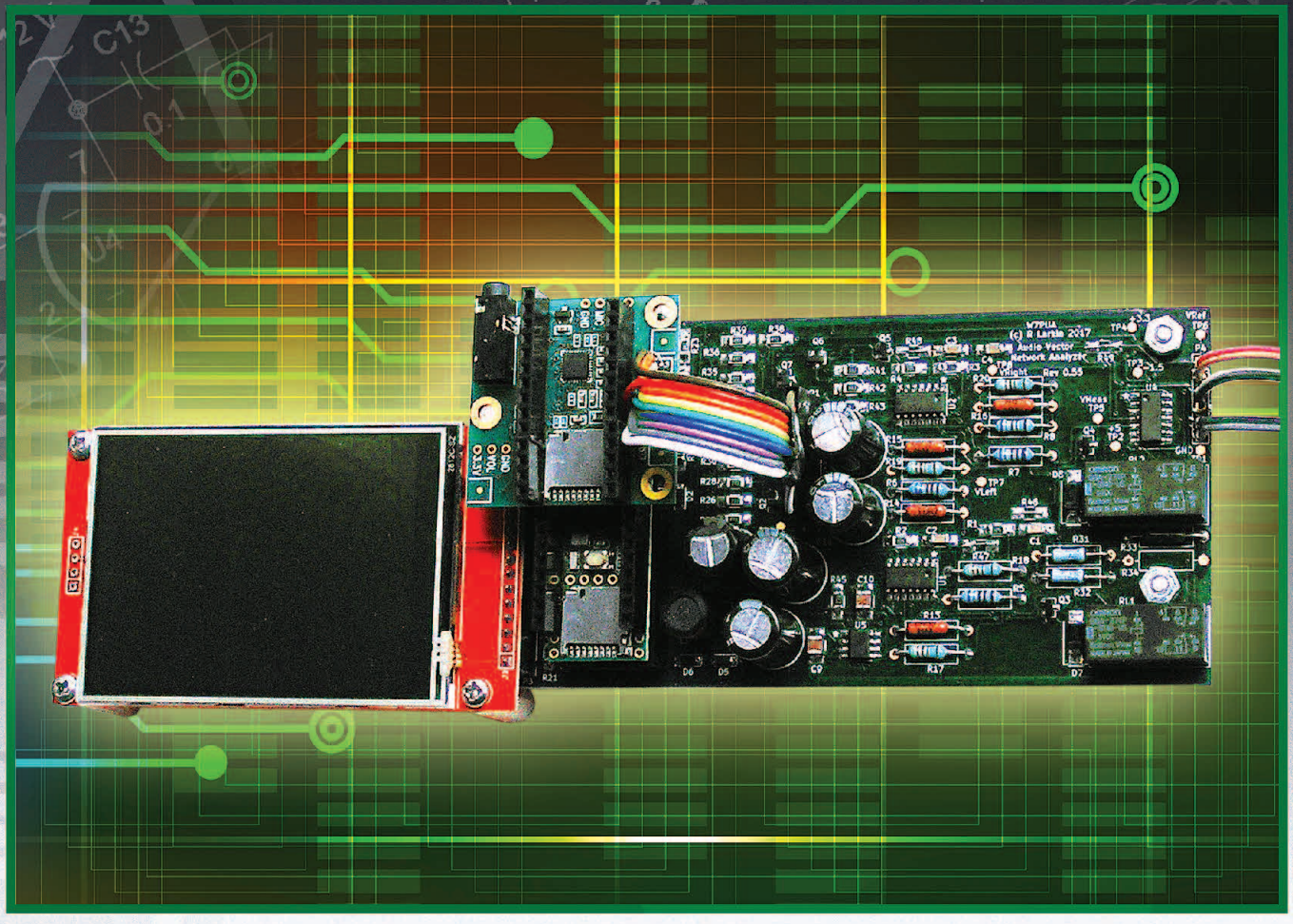

W7PUA describes a DSP-based vector network analyzer for 10 Hz to 40 kHz.

ARRL The national association for AMATEUR RADIO™
225 Main Street
Newington, CT USA 06111-1494

New
APRS® / D-STAR®

TH-D74A 144/220/430 MHz Tribander

Introducing the TH-D74A for the ultimate in APRS and D-STAR performance. KENWOOD has already garnered an enviable reputation with the TH-D72A handheld APRS amateur radio transceiver. And now it has raised the bar even further with the new TH-D74A, adding support for D-STAR, the digital voice & data protocol developed by the JARL, and enabling simultaneous APRS and D-STAR operation – an industry first.

- APRS compliance using packet communication to exchange real-time GPS position information and messages
- Compliant with digital/voice mode D-STAR digital amateur radio networks
- Built-in high performance GPS unit with Auto Clock Setting
- Wide-band and multi-mode reception
- 1.74" (240 x 180 pixel) Transflective color TFT display
- IF Filtering for improved SSB/CW/AM reception
- High performance DSP-based audio processing & voice recording
- Compliant with Bluetooth, microSD & Micro-USB standards
- External Decode function (PC Decode 12kHz IF Output, BW:15 kHz)
- Free software for Memory and Frequency Control Program
- Data Import / Export (Digital Repeater List, Call sign, Memory Channel)
- Four TX Power selections (5/2/0.5/0.05 W)
- Dust and Water resistant IP54/55 standards

APRS (The Automatic Packet Reporting System) is a registered American trademark of WB4APR (Mr. Bob Bruninga).
D-Star is a digital radio protocol developed by JARL (Japan Amateur Radio League).

KENWOOD

Customer Support/Distribution Customer Support:
(310) 639-4200 Fax: (310) 537-8235

www.kenwood.com/usa

JQA-1205 091
ISO9001 Registered
Professional Systems Business Group
JVCKENWOOD Corporation

ADS#29016

QEX

May/June 2018

QEX (ISSN: 0886-8093) is published bimonthly in January, March, May, July, September, and November by the American Radio Relay League, 225 Main Street, Newington, CT 06111-1494. Periodicals postage paid at Hartford, CT and at additional mailing offices.

POSTMASTER: Send address changes to: QEX, 225 Main St, Newington, CT 06111-1494
Issue No 308

Publisher
American Radio Relay League

Kazimierz "Kai" Siwiak, KE4PT
Editor

Lori Weinberg, KB1EIB
Assistant Editor

Zack Lau, W1VT
Ray Mack, W5IFS
Contributing Editors

Production Department

Steve Ford, WB8IMY
Publications Manager

Michelle Bloom, WB1ENT
Production Supervisor

Sue Fagan, KB1OKW
Graphic Design Supervisor

David Pingree, N1NAS
Senior Technical Illustrator

Brian Washing
Technical Illustrator

Advertising Information Contact:

Janet L. Rocco, W1JLR
Business Services
860-594-0203 – Direct
800-243-7768 – ARRL
860-594-4285 – Fax

Circulation Department

Cathy Stepina, *QEX Circulation*

Offices

225 Main St, Newington, CT 06111-1494 USA
Telephone: 860-594-0200
Fax: 860-594-0259 (24 hour direct line)
e-mail: **qex@arrl.org**

Subscription rate for 6 issues:

In the US: $29;

US by First Class Mail: $40;

International and Canada by Airmail: $35

Members are asked to include their membership control number or a label from their QST when applying.

In order to ensure prompt delivery, we ask that you periodically check the address information on your mailing label. If you find any inaccuracies, please contact the Circulation Department immediately. Thank you for your assistance.

About the Cover

Bob Larkin, W7PUA, describes an impedance measuring system with a high accuracy impedance range from 5 Ω to 50 kΩ, and from one-tenth to ten-times that range with reliable good-quality measurements. It is based on the Teensy Arduino microprocessor and covers the 10 Hz to 40 kHz frequency range. It also measures amplitude and phase in transmission mode. A built-in touch screen along with serial control through an USB cable controls the instrument.

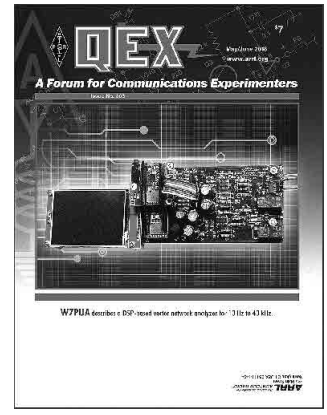

In This Issue

Features

Index of Advertisers

The American Radio Relay League

The American Radio Relay League, Inc, is a noncommercial association of radio amateurs, organized for the promotion of interest in Amateur Radio communication and experimentation, for the establishment of networks to provide communications in the event of disasters or other emergencies, for the advancement of the radio art and of the public welfare, for the representation of the radio amateur in legislative matters, and for the maintenance of fraternalism and a high standard of conduct.

ARRL is an incorporated association without capital stock chartered under the laws of the state of Connecticut, and is an exempt organization under Section 501(c)(3) of the Internal Revenue Code of 1986. Its affairs are governed by a Board of Directors, whose voting members are elected every three years by the general membership. The officers are elected or appointed by the Directors. The League is noncommercial, and no one who could gain financially from the shaping of its affairs is eligible for membership on its Board.

"Of, by, and for the radio amateur," ARRL numbers within its ranks the vast majority of active amateurs in the nation and has a proud history of achievement as the standard-bearer in amateur affairs.

A *bona fide* interest in Amateur Radio is the only essential qualification of membership; an Amateur Radio license is not a prerequisite, although full voting membership is granted only to licensed amateurs in the US.

Membership inquiries and general correspondence should be addressed to the administrative headquarters:

ARRL
225 Main Street
Newington, CT 06111 USA
Telephone: 860-594-0200
FAX: 860-594-0259 (24-hour direct line)

Officers

President: Rick Roderick, K5UR
PO Box 1463, Little Rock, AR 72203

Chief Executive Officer: Barry Shelly, N1VXY

The purpose of *QEX* is to:

1) provide a medium for the exchange of ideas and information among Amateur Radio experimenters,

2) document advanced technical work in the Amateur Radio field, and

3) support efforts to advance the state of the Amateur Radio art.

All correspondence concerning *QEX* should be addressed to the American Radio Relay League, 225 Main Street, Newington, CT 06111 USA. Envelopes containing manuscripts and letters for publication in *QEX* should be marked Editor, *QEX*.

Both theoretical and practical technical articles are welcomed. Manuscripts should be submitted in word-processor format, if possible. We can redraw any figures as long as their content is clear. Photos should be glossy, color or black-and-white prints of at least the size they are to appear in *QEX* or high-resolution digital images (300 dots per inch or higher at the printed size). Further information for authors can be found on the Web at **www.arrl.org/qex/** or by e-mail to **qex@arrl.org**.

Kazimierz "Kai" Siwiak, KE4PT

Perspectives

Mentors

My Amateur Radio mantra is, "Please do your part to lower the average age of hams: Elmer youngsters!" Elmer was personified by David P. Newkirk, W9BRD, in his "How's DX" *QST* column of March, 1971, as a local ham who, "though busy with his own operating, building, arduous studies, chronic family illness, and full social calendar ... miraculously found time to be the big brother to any local youngster or oldster groping uncertainly towards hamdom." Elmer is both a proper noun and an action verb, but the term itself is anachronistic jargon. Times change, and we now prefer *Mentor*!

Consider this. The *QEX* family of hams is aging dramatically. A very recent survey of *QEX* subscribers reveals that about 90% of you, dear readers, are older than 61 years of age, and half of those are over 70. An additional 9% are between 51 and 60 years of age. More than 95% have been licensed for more than 30 years, and nearly two-thirds are retired. What, then, of the future of *QEX*? We need an influx of younger blood — especially between the ages of 40 and 60 — to grow our journal into the near future.

The *QEX* mission is to provide a medium for the exchange of ideas and information among Amateur Radio experimenters, to document advanced technical work in the Amateur Radio field, and to support efforts in advancing the state of the Amateur Radio art. When most of you were at the onset of your ham careers, your main search parameter was "Radio" in your neighborhood library. *QEX* was in its infancy. In contrast, today's generation is immersed in an internet and social media culture. But, you won't find *QEX* there — yet!

Many of your clubs already sponsor ham radio classes and volunteer examiner testing. Please don't stop there. Actively reach out and take the next step. Mentor your newly licensed hams into our fold as *radio-active* hams who can help fulfill the *QEX* mission.

We'd like to hear from you (**qex@arrl.org**), the sages, elders and mentors of Amateur Radio. How can we make the *QEX* mission relevant to the next generations? What can we do to lower the average age of hams? And especially, what can we do to lower the average age of the *QEX* readership?

In This Issue

Our *QEX* authors contributed to the communications experimental arts in diverse Amateur Radio topics.

Ulrich L. Rohde, N1UL and Ajay K. Poddar, AC2KG, study the phase noise and frequency stability in an optimized grounded-base VHF and UHF oscillators.

Matthew H. Reilly, KB1VC, introduces the Arduino ecosystem, which includes a wide variety of easy-to-use integrated hardware components, and software development environment.

Bob Larkin, W7PUA, reveals an impedance measuring system based on the Teensy Arduino microprocessor, that also measures amplitude and phase in transmission mode.

John Stensby, N5DF, describes how to make a better RF voltmeter probe.

Keep the full-length *QEX* articles flowing in, but if brevity is your forte, share a brief **Technical Notes** of perhaps several hundred words in length plus a figure or two. Expand on another author's work and add to the Amateur Radio *institutional memory* with your technical observation. Let us know that your submission is intended as a **Note**.

QEX is edited by Kazimierz "Kai" Siwiak, KE4PT, (**ksiwiak@arrl.org**) and is published bimonthly. *QEX* is a forum for the free exchange of ideas among communications experimenters. The content is driven by you, the reader and prospective author. The subscription rate (6 issues per year in the United States is $29. First Class delivery in the US is available at an annual rate of $40. For international subscribers, including those in Canada and Mexico, *QEX* can be delivered by airmail for $35 annually. Subscribe today at **www.arrl.org/qex**.

Would you like to write for *QEX*? We pay $50 per published page for articles and Technical Notes. Get more information and an Author Guide at **www.arrl.org/qex-author-guide**. If you prefer postal mail, send a business-size self-addressed, stamped (US postage) envelope to: *QEX* Author Guide, c/o Maty Weinberg, ARRL, 225 Main St, Newington, CT 06111.

Bob Larkin, W7PUA

2982 NW Acacia Place, Corvallis, OR 97330; **w7pua@arrl.net**

DSP-Based Vector Network Analyzer for 10 Hz to 40 kHz

This impedance measuring system, based on the Teensy Arduino microprocessor, also measures amplitude and phase in transmission mode. Control is by built-in touch screen along with serial control through a USB cable.

Network analyzers at RF frequencies have become popular with amateur experimenters. In one form, the "antenna analyzer" is available commercially and often can measure both resistive and reactive components of an impedance. In its more sophisticated form, measurements can also be made of transmission circuits, such as filters. Examples of the latter are the N2PK[1] and DG8SAQ[2] Vector Network Analyzers (VNA). My experience with the N2PK design included many fine measurements, but sometimes the lower frequency limit of about 50 kHz left a need. Note that the DG8SAQ design operates down to about 1 kHz.

Several interesting approaches to these measurements have been published. The project from George Steber, WB9LVI,[3] measures impedances in the audio range with a minimal amount of hardware along with a PC sound input. The huge advantage of this is hardware simplicity, but it does not provide for a wide range of frequencies nor transmission measurements. Jacques Audet, VE2AZX's Low-Frequency Adapter[4] is very flexible, but requires an RF VNA.

I became curious about making a parallel design to the RF VNA using DSP. The goal was a VNA that would cover from perhaps 10 Hz to a frequency that would join up with the N2PK VNA coverage. I hoped that most of the complexity could be hidden in software and in doing so, the cost could remain low. When fellow experimenter, Johannes Forrer, KC7WW, steered me towards the Teensy Arduino DSP-capable product[5], I was on my way.

The original idea was to make this Audio Vector Network Analyzer (AVNA) a USB serial driven box without a front control panel. But the availability of the 320x240 color touch screen at low cost[6] changed the approach. The final AVNA has serial control as well as a touch-screen fully-independent alternative. This is very convenient for component identification and measurements, in particular. The stand-alone capability includes transmission as well as swept measurements, there is no need to use the complete PC control.

The result is a little box, costing around US$100, that can do conventional VNA functions and also serves as an LCR meter for resistors from a fraction of an ohm up to a few megohms, capacitors from a picofarad up to thousands of microfarad, and inductors from a few nanohenry up to thousands of henry.

To make this project available to as many experimenters as possible, high quality double-sided printed circuit boards have been made available, in multiples of 3, through OSH Park[7]. The software is open-source[8], as is the development system[9] and the processor/CODEC library software[10].

Overall Operation

The block diagram of Figure 1 shows how a combination of hardware and software produces a conventional VNA. The process starts with a sine wave generator implemented as direct numerical calculation in DSP software. This signal can be at any frequency from 10 to 40,000 Hz and is sent to a Digital-to-Analog converter (DAC) that drives an amplifier producing a very low output impedance. Relays are used to connect a precision resistor of either 50 or 5 kΩ to the impedance measurement point. This resistor is used as a reference for measuring impedances, and also serves as a known source resistance for transmission measurements. If desired for transmission measurements, the low output impedance point can also be accessed directly.

Both impedance and transmission measurements involve knowing the amplitude and phase of the sine wave voltage at the low-impedance output. This is the reference signal, and it is always available via the right channel Analog-to-Digital Converter (ADC). The left channel measurement is taken across the unknown impedance for impedance measurements, or at the output of the device being tested for transmission measurements. Differential Op-amps ahead of the ADC allow careful control of their megohm input impedance. This allows software correction of this quantity when measuring impedance.

Inside the DSP, the two outputs of the ADCs are each applied to a pair of mixers that are multipliers. Each pair of multipliers has a locally generated sine and cosine wave for producing in-phase, *I*, and quadrature, *Q*, measurements. This process is completely analogous to direct-conversion receivers. Implemented in DSP, the isolation between either of the inputs and the output is close to perfect. The output signal does still include second harmonics of the inputs, that are

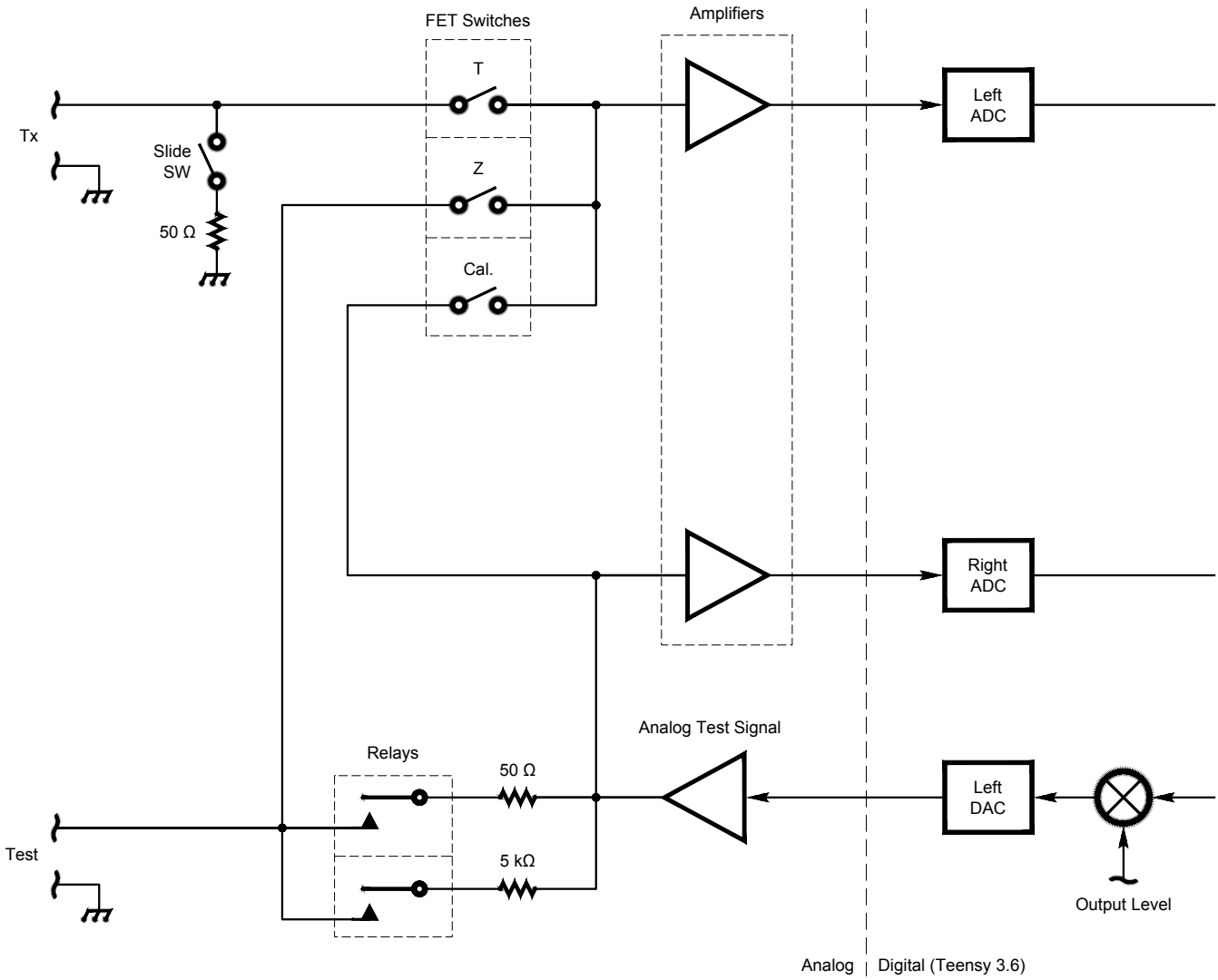

Figure 1 — Block diagram shows a sine wave signal source that comes from the DSP via the left DAC. One of the two receiving channels always measures this signal level via the right ADC and is the reference channel. The left ADC measurement channel is switched between three functions, Calibrate, Impedance, and Transmission. Two different reference resistors can be selected by relays to provide either 50 or 5,000 Ω test level.

important and will be discussed below.

Next, the *I* and *Q* signals for the reference and measurement channels are averaged over at least a tenth of a second to reduce noise and increase the range of signal levels over which accurate measurements can be made. In the DSP, the averaged *I* and *Q* are converted to amplitude and phase by calculating

$$\text{amplitude} = \sqrt{I^2 + Q^2} \;;$$

$$\text{phase} = \arctan\left(Q/I\right)$$

Error corrections applied at this point correct for gain and phase differences in the measurement and reference amplifiers, as well as for the input impedance of the measurement amplifier. Finally, for impedance measurements, the resistance and reactance of the unknown component is found from the voltage amplitudes at the top of the reference resistor and across the unknown impedance, along with the relative phase shift. For transmission measurements the gain or loss comes directly from the measurement of the input and output.

The basic structure of this VNA is parallel to that of RF tools such as the N2PK VNA. Sine waves are computed in the DSP rather than by lookup tables in a DDS. Multipliers are mathematical operations in DSP rather than MC1496 Gilbert cell devices. One area that is a bit different is the impedance measurement method. The most common device for the RF frequencies is a bridge, comprised of three precision resistors and a transformer to keep grounds isolated. This can be implemented at low frequencies as well, but the accuracy and simplicity of measurements using a single reference resistor favor this latter method. To some extent, this method also has a parallel. The N2PK project has an *I-V* accessory board available[11] that extends this single reference method to RF, using a pair of high turns-ratio transformers.

Hardware

The schematic diagram of the AVNA hardware PC board, Figure 2, shows the processor board, U3. This is not an IC, but rather the Teensy 3.6 version of an Arduino. Not shown is the PJRC Audio Adapter ADC/DAC board that plugs directly into Teensy

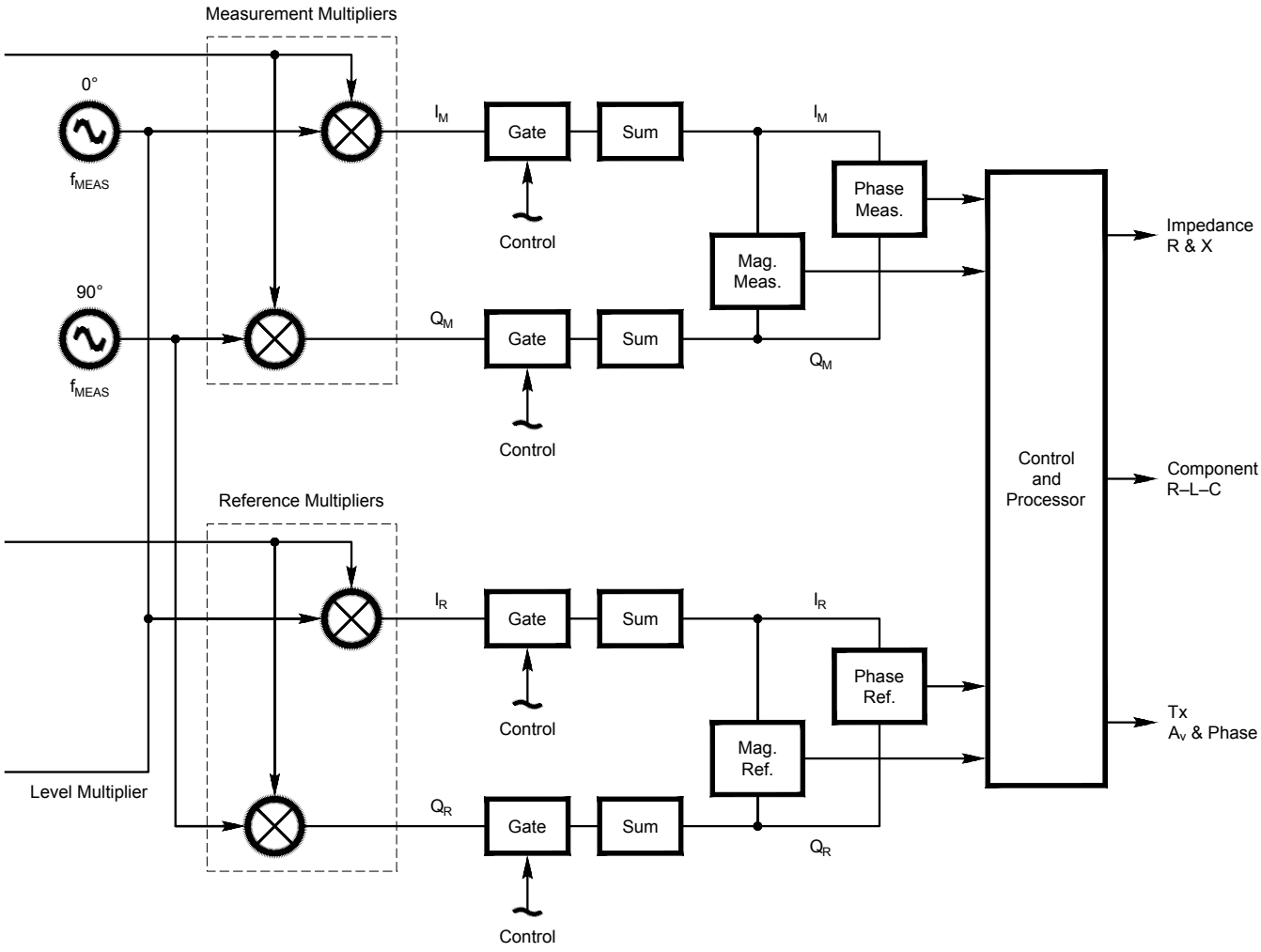

board[12] and connects to the AVNA board via P1. The Teensy board is a member of the Arduino family. Its software allows most of the Arduino IDE and library programs to be applied. To the user it behaves like an Arduino. However, the processor and memory capabilities are much greater than a board such as the Arduino UNO[13]. The Teensy 3.6 uses an ARM Cortex-M4 processor with a basic instruction rate of 180 MHz, an internal 32-bit floating-point processor, and a considerable instruction set just for DSP, see the sidebar "DSP Code in Teensy Arduino". Part of the Teensy board is a USB serial interface that allows full control of the AVNA from most computing devices such as PCs and Laptops.

Not shown on the schematic is the front panel device which is a 320x240-pixel color LCD with touch-screen capability. This plugs into P3 on the AVNA board, either directly or with an extension cable. This display provides a stand-alone capability for the AVNA.

The amplifier comprising U1B op-amp and the transistors Q1 and Q2 has no voltage gain but, because of heavy negative feedback, provides both power drive and a low output impedance. One of a pair of relays, RL1 and RL2, connects the Unknown Z output connector to the drive voltage. These relays were chosen because their gold contacts help to ensure a reliable output impedance. The impedance setting resistors, R31, R32 and R33, R34, are parallel combinations that can be used in several ways to provide accurate 50 and 5 kΩ values. As shown, a single 50 Ω 0.05% resistor and a pair of 10 kΩ 0.05% resistors are used. These high precision resistors are used for their low 10 ppm temperature coefficients. Errors in the resistor values can be calibrated out in the software. Any other combination of parallel resistors can be used, depending on what you have available.

Three FET switches, parts of U4, choose the input path for the measurement channel. The calibrate switch, U4B, connects the reference and measurement channel inputs together. With both relays open, this provides an accurate measurement of the differences in gain and phase between the two channels. These differences are small, but end up distinguishing between rough measurements

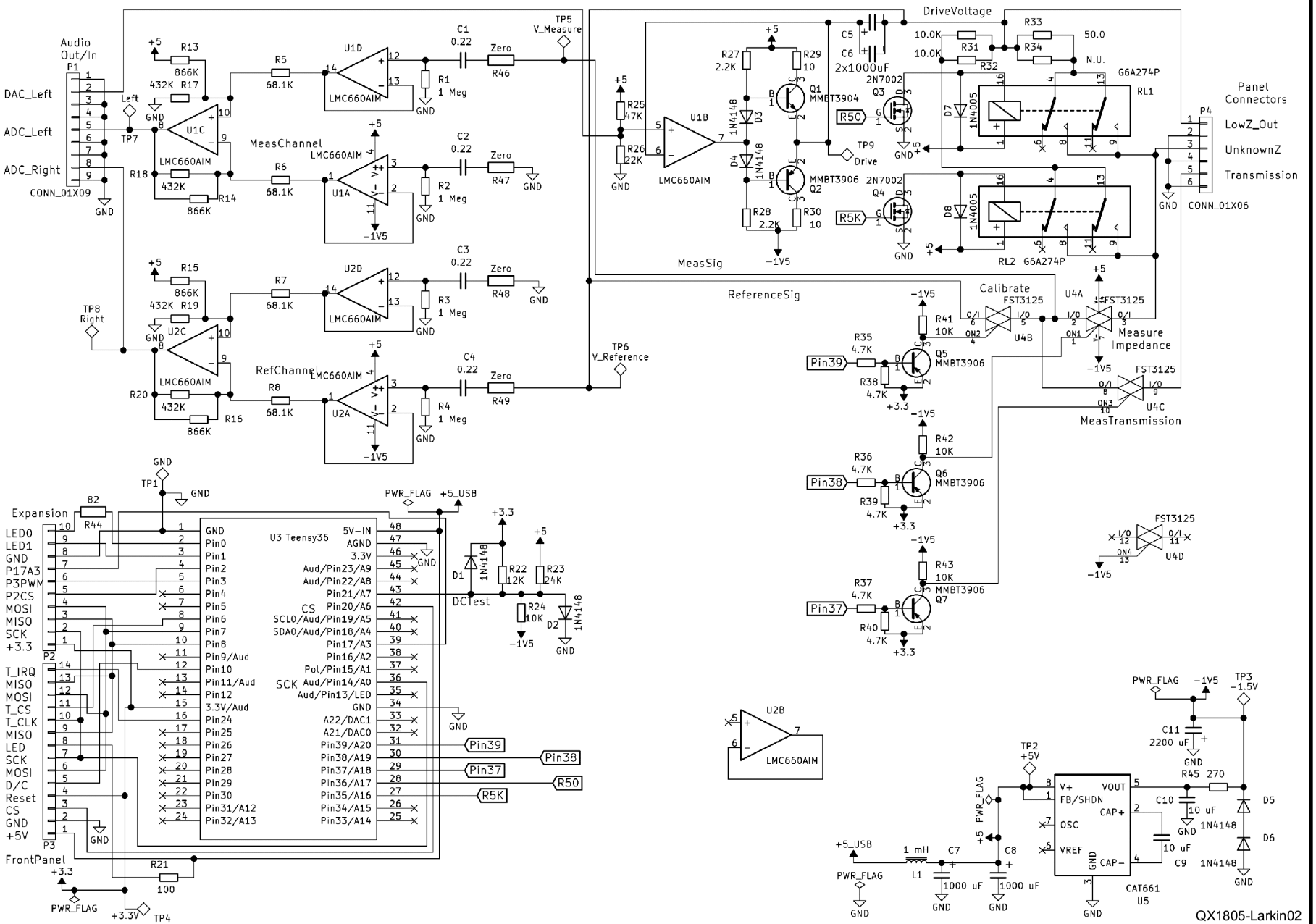
Audio Out/In
P1
DAC_Left
ADC_Left
ADC_Right
CONN_01X09
Left
TP7
U1C
U1D
U2C
U2D
U1A
U2A
LMC660AIM
MeasChannel
RefChannel
R13
866K
R17
432K
R18
R14
R5
R6
R15
R19
R20
R16
R7
R8
68.1K
C1
C2
C3
C4
0.22
Zero
R46
R47
R48
R49
R1
R2
R3
R4
1 Meg
TP5
V_Measure
TP6
V_Reference
TP8
Right
U1B
R25
47K
R26
22K
R27
2.2K
R28
R29
10
R30
D3
D4
1N4148
Q1
MMBT3904
Q2
MMBT3906
TP9
Drive
DriveVoltage
C5
C6
2x1000uF
R31
R32
R33
R34
10.0K
50.0
N.U.
Q3
Q4
2N7002
R50
R5K
D7
D8
1N4005
RL1
RL2
G6A274P
P4
Panel Connectors
LowZ_Out
UnknownZ
Transmission
CONN_01X06
MeasSig
ReferenceSig
Calibrate
FST3125
U4A
U4B
U4C
U4D
Measure Impedance
MeasTransmission
R41
10K
R35
4.7K
R38
R42
R36
R39
R43
R37
R40
Q5
Q6
Q7
Pin39
Pin38
Pin37
+3.3
-1V5
Expansion
P2
P3
FrontPanel
LED0
LED1
P17A3
P3PWM
P2CS
MOSI
MISO
SCK
T_IRQ
T_CS
T_CLK
LED
D/C
Reset
CS
R44
82
R21
100
U3 Teensy36
5V-IN
AGND
3.3V
Aud/Pin23/A9
Aud/Pin22/A8
Pin21/A7
Pin20/A6
SCL0/Aud/Pin19/A5
SDA0/Aud/Pin18/A4
Pin17/A3
Pin16/A2
Pot/Pin15/A1
Aud/Pin14/A0
Aud/Pin13/LED
A22/DAC1
A21/DAC0
Pin39/A20
Pin38/A19
Pin37/A18
Pin36/A17
Pin35/A16
Pin34/A15
Pin33/A14
Pin0
Pin1
Pin2
Pin3
Pin4
Pin5
Pin6
Pin7
Pin8
Pin9/Aud
Pin10
Pin11/Aud
Pin12
3.3V/Aud
Pin24
Pin25
Pin26
Pin27
Pin28
Pin29
Pin30
Pin31/A12
Pin32/A13
TP1
TP4
PWR_FLAG
+5_USB
D1
D2
DCTest
R22
12K
R23
24K
R24
10K
U2B
TP2
TP3
-1.5V
C11
2200 uF
R45
270
C10
10 uF
C7
C8
C9
1000 uF
L1
1 mH
CAT661
U5
VOUT
FB/SHDN
CAP+
OSC
VREF
CAP-
D5
D6
QX1805-Larkin02

Figure 2 — Schematic diagram of the AVNA PC board.The relays are small signal with gold-plated contacts, Omron G6A-274P-ST40-US-DC5 (DigiKey Z2931-ND)]. Resistors R31 and R32 are 0.05%10 kΩ with 10 ppm/°C temperature coefficients (Mouser 594-UXB02070F1002AR1). R33 is 50 Ω (Mouser 71-PTF5650R000AYR6).

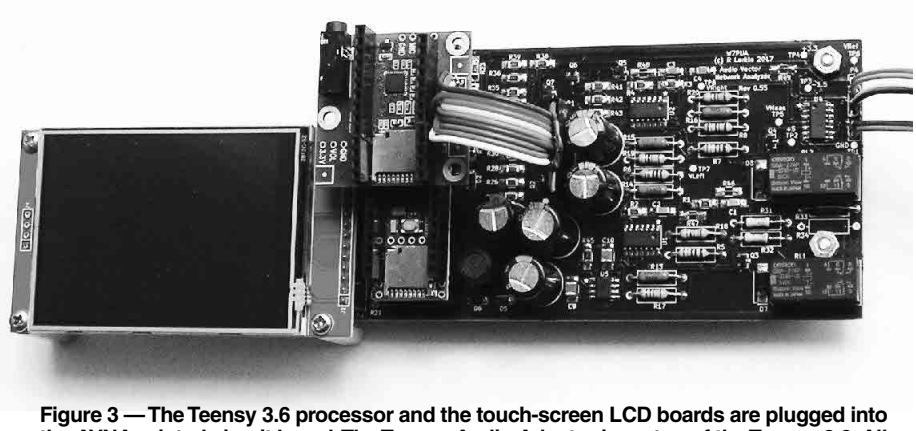

Figure 3 — The Teensy 3.6 processor and the touch-screen LCD boards are plugged into the AVNA printed circuit board. The Teensy Audio Adaptor is on top of the Teensy 3.6. All precision resistors are leaded types.

and those of a precision instrument. Because of the relays, this calibration can be done with components connected to the measurement connector. Switches, U4A and U4C, connect the measurement channel for either impedance or transmission measurements.

The reference and measurement channels have identical amplifiers driving the pair of ADCs. The voltage gain of about 3.7 allows the drive voltage to be delivered from the linear region of the output amplifier. This gain can sometimes increase the dynamic range of transmission measurements. The amplifiers should be matched so that the two sides of the differential amplifier should be the same. To this end, I purchased a surplus of resistors in values for R5 to R8, R13 to R16, and R17 to R20, and selected a matched sets of four. The exact values are not important. I used leaded 50 ppm temperature coefficient resistors. The 0 Ω resistors at the amplifier inputs, R46 to R49, are not required for the AVNA, but allow for future experimentation.

The AVNA is supplied by the 5 V dc on the USB cable going to the Teensy board. Current consumption is about 200 mA, allowing operation from any USB power source, including rechargeable battery types. The -1.5 V supply is needed to increase the voltage swing of the DAC output amplifier, and is produced by the CAT661 switched-capacitor voltage inverter, U5. The 3.3 V supply is on the Teensy board. The three supply voltages, 5, 3.3 and -1.5 V, are monitored by the Teensy using a single analog voltage input generated by resistors R22 to R24.

The Teensy 3.6 board has a large number of inputs and outputs supported by peripheral controllers for a wide variety of devices. Many of these pins are unused in the AVNA and could be used to expand the functions of this project. Likewise, the project uses just a small part of the available memory for programs and data.

Overall Assembly

Most of the assembly is done by merely plugging the Teensy board into the AVNA board and plugging the Teensy Audio Adapter into the Teensy board. Orientation of the connectors is important, see Figure 3. The LCD+Touch-Pad board likewise will operate

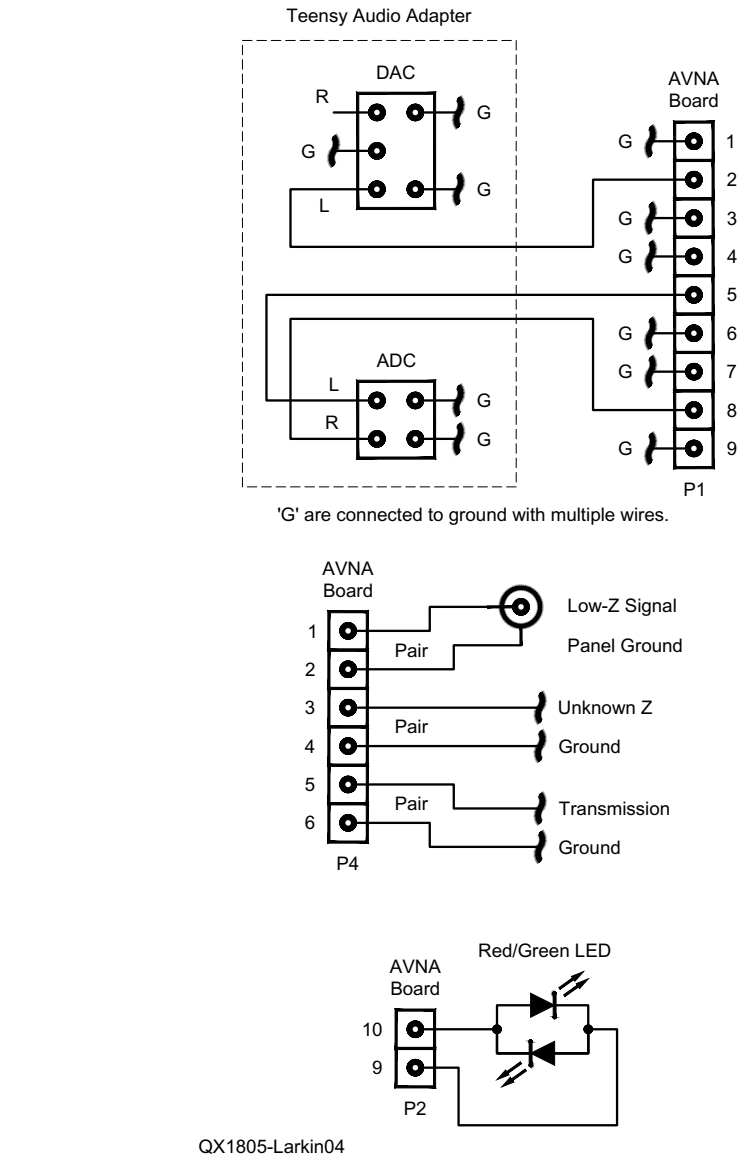

Figure 4 — This diagram shows the interconnection that requires wiring, rather than plugging boards together. All connections except for the LED carry audio signals and use multiple ground leads to minimize ground loops and capacitive coupling. The "Unknown Z" and "Transmission" terminals keep the ground isolated from the panel for the same reason. The LED is red/green bi-color, and the connector can be reversed if green is not the normal color.

by plugging it directly into the AVNA board at P3. If this is done, the LCD ends up physically lower than the Audio Adapter. With a bit of extra effort, a step can be put into the top of the enclosing box, giving full access to the LCD. I did this for the wooden box shown in Figures 7 and 12. Alternatively, an extension cable can be placed on the touch-screen, allowing a simpler package.

Figure 4 shows the wiring that is external to the PC boards. My construction used banana plug terminals for the Impedance and Transmission panel connections, but these could be coaxial connectors. The "Low-Z" output from the drive voltage is for specialized transmission measurements, and not normally used. For convenience I brought this to a BNC connector. Not shown in this figure are the interconnections between the Teensy 3.6 board and the other parts. These can be seen on the Figure 2 schematic for the AVNA board.

The AVNA starts up as soon as power is applied to the USB connector on the Teensy board. This USB connector can carry serial data, or for stand-alone operation, it can merely supply power from any standard USB power source. The connector is a USB Micro-B style. The schematic shows P2, listed as an expansion connector. This has no particular function at present, but does make available an I2S serial interface, as well as analog and general purpose digital pins.

DSP Functions

All measurements are made using the two analog inputs, labeled as *Reference and Measurement* channels. The digital outputs from the ADC are 16-bit signed words. ADC noise covers several of these bits, not all of which is random. The coherent portions of the ADC noise can be avoided by careful choice of sampling frequencies. For this reason, both 44.1 kHz and 100 kHz sampling rates are used, as automatically set in the software. The 100 kHz sampling rate allows measurement frequencies up to about 40 kHz. This is high enough to have adjoining ranges with the N2PK VNA. The lower end of measurement frequencies is set at 10 Hz by the coupling capacitors that are on the Teensy Audio Adapter. These could probably be changed, and along with a few other modifications, to allow operation below 10 Hz.

Referring back to the block diagram, the digital outputs of the ADC are applied to multipliers. A bit of trigonometry shows us most of what we need to understand the operation. The internally generated sine wave at frequency f Hz is $\sin(2\pi ft)$, where t is time in seconds. This waveform is centered around zero volts and has maximum excursions of ±1. Our reference or measurement signals are exactly the same frequency, but with amplitude A and phase shift p,

$$A\sin(2\pi ft + p)$$

Applying trigonometric identities to the product of our sine waves, we find the multiplier output voltage is of the form,

$$e_{os} = \frac{A}{2}\cos(p) - \frac{A}{2}\cos(2\pi 2ft)$$

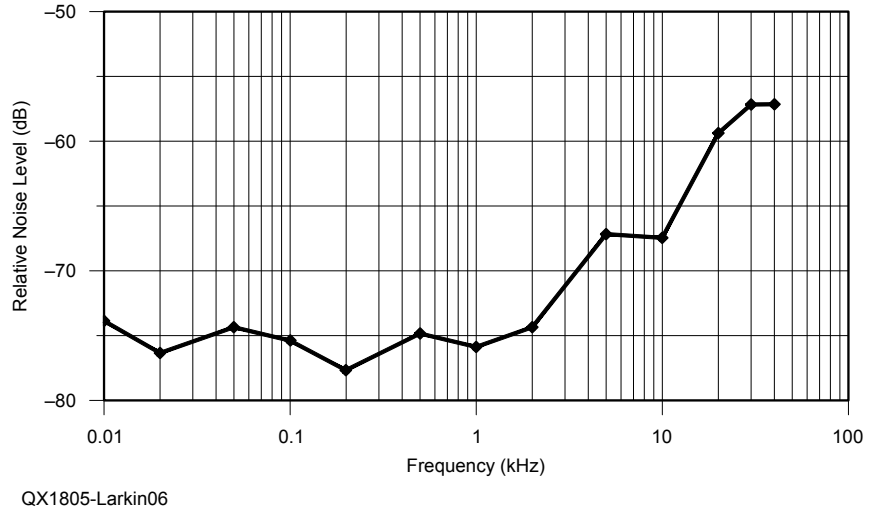

Figure 6 — Response of a transmission measurement with no connection to the input, except for the 50 Ω termination. The floor is 75 dB below full input up to 2 kHz, then rises with increasing frequency. The rise is due to capacitive leakage in the "Calibrate" FET switch.

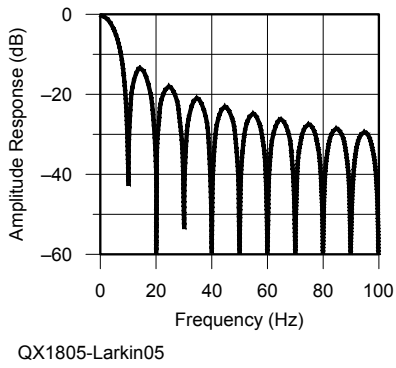

Figure 5 — Frequency response is averaged for a tenth of a second. The position of the nulls can be set exactly by controlling the length of the averaged sample period. The nulls for this tenth second average occur at 10 Hz intervals at and above 10 Hz. This eliminates the second harmonic output from the multipliers.

Figure 7 — The AVNA shows the measurement of a 20 nF capacitor at 2,000 Hz.

which shows that the output of the multiplier has no component at the fundamental frequency *f*. The first term is an output at dc, which is the desired value. The second term is at the second harmonic 2*f*, which we don't want. Because of the low frequency involved, we do the low-pass filtering to eliminate the second harmonic by averaging the multiplier output over a very specific period of time. If averaging period is an integer multiple of the second harmonic period, the harmonic component will always cancel out completely, independent of the phase of the harmonic signal. The AVNA uses 64-bit double-precision floating point for this averaging to prevent loss of resolution. The averaging time period must be at least a full cycle at 20 Hz, or 50 ms. The current implementation uses averaging times of around 0.1 second, or two periods at 20 Hz. The exact averaging time depends on the measurement frequency. Depending on the frequency of operation, a slight adjustment of the measurement frequency may be needed to account for the inflexible 44,100 or 100,000 Hz. sample rate.

This averaging process can be viewed as a finite impulse response (FIR) low-pass filter. The FIR coefficients are all the same value and the number of FIR taps is that required to span an integer number of second harmonic cycles. The frequency response of this low-pass design is of the general form,

$$\frac{\sin(kf)}{f}$$

and a careful choice of *k* can place nulls at the second harmonic frequency. The integer second harmonic approach described above is one easy way to choose a proper *k*. The frequency response of the averaging is shown in Figure 5 for the 0.1 second averaging time suitable for use at 5 or 10 Hz.

The in-phase and quadrature components *I* and *Q* can be handled computationally as complex numbers, $I + jQ$, where *j* is the square root of -1. The Arduino system, through its underlying C++ language, easily handles calculations with complex numbers without separating the real and imaginary parts. Examination of the program shows that this is used extensively.

Getting back to finding the measured impedance, the complex voltages from the measurement and reference channels are corrected for small amplitude and phase errors. Next the measured impedance complex value $Z_m = R + jX$, is found from the voltages by

$$Z_m = R\frac{V_m}{V_r - V_m}$$

That is, the complex voltage across the reference resistor is proportional to the complex current flowing through it. The unknown impedance is then the complex voltage across the unknown, divided by the current. This is the total impedance across the measurement point and includes the components at the input to the amplifier. The input circuitry needs to be de-embedded mathematically. The input components, R1, C1, the input stray capacity, lead inductance and lead resistance are all compensated for. These values remain relatively fixed with a particular measurement configuration, so the AVNA needs no procedure for automatically calibrating these values. If needed, they can be changed by commands from a PC.

The DSP functions described here are all part of the Arduino sketch using the Teensy audio library. This hides away many of the bookkeeping details of grouping ADC input samples into blocks and having the data blocks handled in the proper order. The necessary data hooks are all available to interface with conventional Arduino C++ functions. In addition, the hardware floating-point operations are all available to the sketch. In some places, it is useful to have full double-precision calculations. For this, slower software routines are all available. The Arduino development environment remains conventional for all of this. It has proven to be a convenient and powerful set of tools.

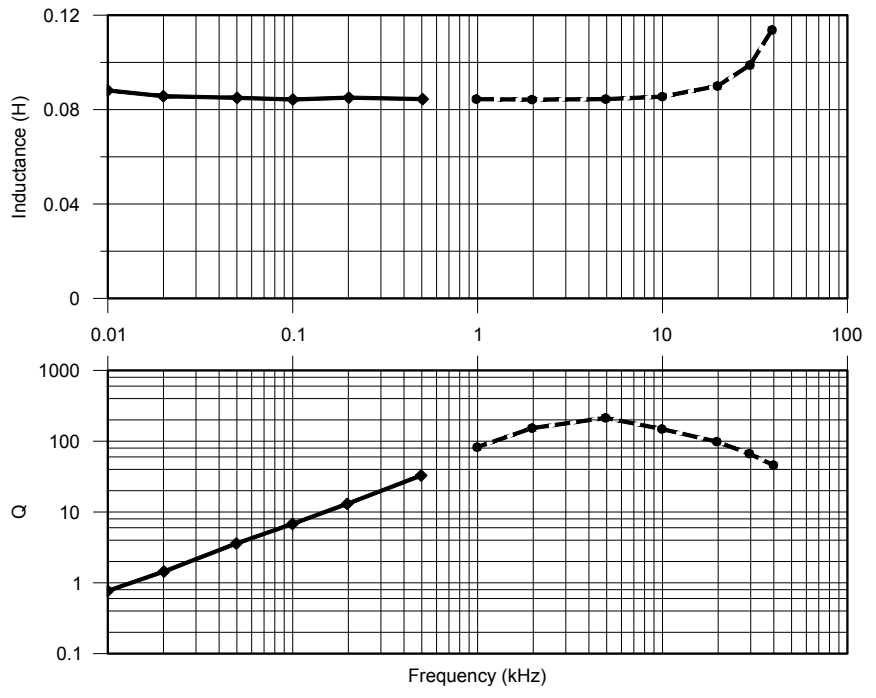

Figure 8 — Measurements of the inductance and Q of an 88 mH inductor below 1,000 Hz were made with a 50 Ω reference resistor, while the higher frequency measurement used the 5 kΩ reference. The rise in apparent inductance above 10 kHz is attributed to the shunt capacitance of the inductor.

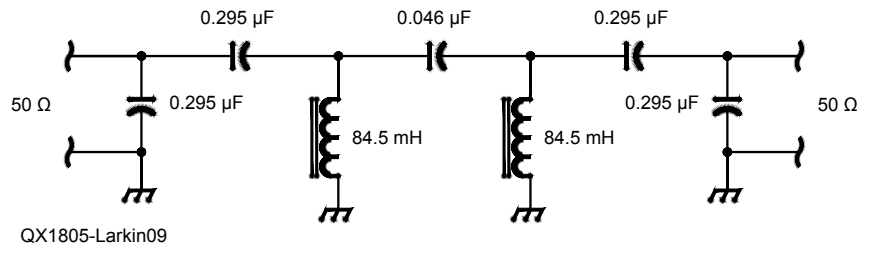

Figure 9 — Schematic of a double-tuned filter test piece designed around available components.

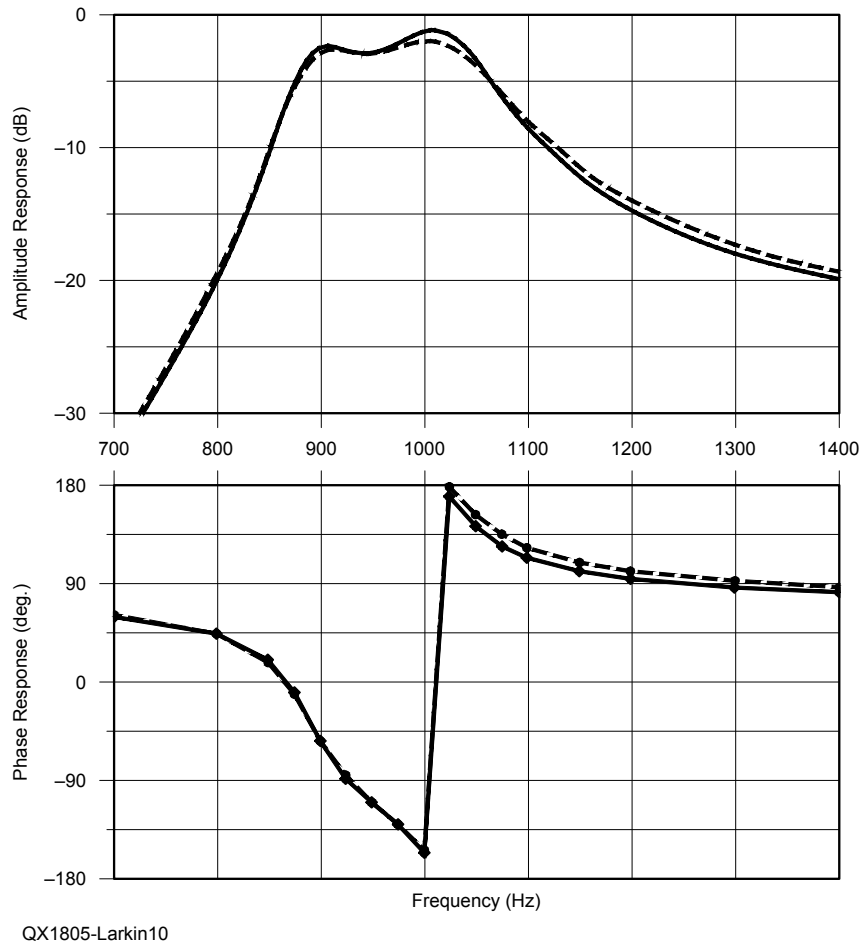

Figure 10 — The amplitude and phase response for the 2-inductor filter of Figure 9. The dashed line shows the computer-predicted response, based on the measured inductor impedance. The solid line shows the AVNA measured response of the completed filter.

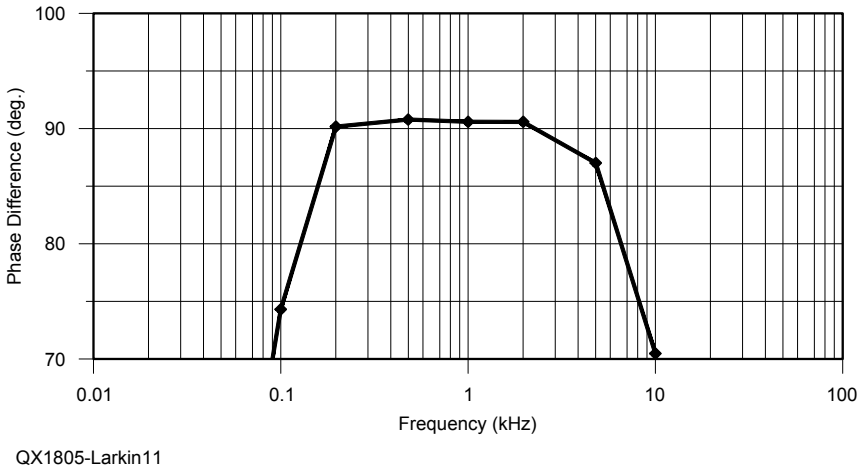

Figure 11 — The transmission function was used to measure the response of a Mini-R2 phasing receiver. Separate measurements were made of the phase-shift of the two receiver channels, and the difference is shown here.

Control of the AVNA

A large part of the Teensy program is devoted to control functions. This is done twice since control from the touch-screen and from a PC via the serial connection are usually different in detail. For direct display, the emphasis is on convenience of making measurements. This limits the options somewhat, as does the size of the display. The serial control is intended to work with a program in a PC and thus flexibility is important.

With touch-screen control, a measured impedance can be displayed in a number of ways:

- Series resistance and reactance (*R* and *X*)
- Series inductance or capacitance, and *Q*
- Parallel resistance and reactance
- Parallel inductance or capacitance, and *Q*.

The best choice depends on the component being measured and the application. There are always six annotated buttons at the bottom of the display to control functions.

For transmission measurements the touch-screen display shows gain both as a voltage ratio and in dB, along with the phase shift in degrees.

In addition to measuring components at a single predetermined frequency, a 13-frequency broad-band sweep is always available. This covers 10 Hz to 40 kHz in 1-2-5 steps, see points in Figure 8. There is sufficient touch-screen space for 7 results, which can be scrolled to cover any of the 13 frequencies. This same sweep is also available for transmission measurements.

Available only from touch-screen is a "What?" function that does two impedance sweeps with 50 and 5 kΩ references. An estimate of the measurement quality is made by the observed impedance magnitude. For the best quality measurement the component value, such as "*L* = 2.5 mH *Q* = 8.6", is displayed. In addition, a rough quality estimate is given in terms of excellent, good, poor and no value. For many purposes, this gives a quick evaluation of components with minimal setup.

The control from a PC uses about 25 commands. A typical command is "FREQ 1251" that sets the generator and detectors to 1251 Hz.

Impedance Measurement Accuracy

Standard components to measure against are a perfect way to check for accuracy. Ideally one should have a bag full of 0.1% *R*, *L* and *C* components. For most of us, this is not the case, especially for *L* and *C* parts where the best tolerances available at experimenter prices are about 2% for *L* and 1% for *C*. At mid-range component values,

the precision of this AVNA is better than the accuracy of these available comparison *L* and *C* values. This leads to a conclusion that impedance measurements done with this instrument are probably better than the available reference parts. This instrument topology fundamentally references reactance measurement back to a single resistor. Resistors with 0.1% or 0.05% tolerance are readily available, and also many people have access to a high accuracy Digital Voltmeter-Ohmmeter. The AVNA part list has the 50.0 and 5,000.0 Ω resistors known to within 0.05%.

A first check of the final board was to measure resistance. I used the rule: measure impedances over the level of 500 Ω with the 5 kΩ reference and those below with the 50 Ω reference. The Table 1 results were obtained at 1,000 Hz.

The best accuracy is for values near the reference resistors. Accuracy analysis of the measurement circuit predicts that. The larger errors for measuring values are around a megohm, and may come from not having the proper compensating value in software for the R1 input resistor.

Moving to the next best known component, the capacitor, we obtained the results in Table 2, at frequencies where the reactance was in the same order of 500 Ω. These capacitor measurements show the general range of errors around the central impedance ranges. The last measurement included subtracting the 1.3 pF that was showing with no component attached.

One area where it is useful to explore inductance measurements is for small coils at 40 kHz. Here we have inductors that have Q-meter and RF network analyzer measurements. For example, 18 turns of #26 squeezed together on a T37-6 toroid shows 1.61 µH at 7.9 MHz on a Boonton Radio 260-A Q-meter, and 1.59 µH at 40 kHz with an N2PK VNA. At 40 kHz this inductor measured 1.65 µH using the AVNA.

One final accuracy test example is a 0.47 µF, 1% capacitor in series with a 5,000 Ω, 0.05% resistor. At 500 Hz, this measures 0.4769 µF in series with a 4998 Ω resistor, in good agreement with the separate measurements.

Figure 12 — The AVNA screen shows the result of using the "What?" function to determine the best measurement of a Pi inductor marked as 50 µH, using the 50 Ω and 5 kΩ reference resistors. The quality grade is shown on the right edge, with "E" meaning excellent, and "P" for poor. The value of this inductor allows it to have excellent quality with 50 Ω and at 40 kHz. Other quality grades are "G" for good and "0" for don't use.

Table 1

Measured resistor	*AVNA value*	*Difference*	*Difference*
10.000 ± 0.005 Ω	9.975 Ω	-0.025 Ω	-0.250%
50.000 ± 0.025 Ω	50.018 Ω	+0.018 Ω	+0.036%
100.00 ± 0.05 Ω	99.90 Ω	-0.10 Ω	-0.100%
5,000.00 ± 0.25 Ω	4998.7 Ω	-1.3 Ω	-0.026%
20,000.0 ± 10 Ω	19918 Ω	-82 Ω	-0.410%
100.0 k ± 50 Ω	99330 Ω	-670 Ω	-0.670%
1.00 M ± 500 Ω	973,000 Ω	-27,000 Ω	-2.70%

Table 2

Ref R Ω	*Frequency*	*Capacitor*	*Measured*	*Difference*	*Difference*
5 k Ω	500 Hz	0.470 ± 0.0047 µF	0.4715 µF	+0.0015 µF	+0.32%
50 Ω	500 Hz	0.470 ± 0.0047 µF	0.4684 µF	-0.0016 µF	-0.34%
5 k Ω	200 Hz	0.940 ± 0.0094 µF	0.9442 µF	+0.0042 µF	+0.45%
50 Ω	200 Hz	0.940 ± 0.0094 µF	0.9265 µF	-0.0135 µF	-1.44%
50 Ω	2,000 Hz	0.01 ± 0.,0001 µF	0.00993 µF	-0.00007 µF	-0.70%
5 k Ω	2,000 Hz	0.01 ± 0.,0001 µF	0.00999 µF	-0.00001 µF	-0.10%
5 k Ω	40,000 Hz	100.0 +/-1.0 pF	99.5 pF	-0.5 pF	-0.50%

Transmission Accuracy

The calibration for transmission measurements involves two steps. First, the measurement and reference channels are made to track by comparing their response with the inputs tied together by the "*Calibrate*" switch U4B. Next, the transmission path is normalized for external components by doing transmission measurements with a through-path in place. Amplitude and phase values are stored for later forming of ratios and subtractions.

As a quick check on transmission, a re-measurement was done with the through-path still in place. This typically shows amplitudes between 0.9999 and 1.0001 and phase errors around 0.02°, which is the noise in the system.

A simple *RC* circuit, consisting of a series resistor followed by a capacitor to ground, was used to test the transmission path. An external 5,000 Ω, 0.05% resistor was in series with the internal 50 Ω source resistor. A 0.02 µF, 1% capacitor was connected across the high-*Z* measurement port. The response of this circuit can be easily calculated to allow a comparison with the measured values. The most telling measurement is probably the phase shift around the 45° phase shift point of 1576 Hz (for exact component values). The calculated and measured phase shifts differed by 0.14° at 1,000 and 2,000 Hz, and could be fully matched by changing the calculated capacitor to 0.019905 µF. The capacitor value difference is about 0.5%, which seemed reasonable.

A limiting factor for transmission measurements is the noise floor and transmission feed-through. These cause an

apparent output when no input is applied. Figure 6 is a swept plot with the input shunted by 50 Ω. Noise limits the dynamic range to about 75 dB up to about 2,000 Hz. At higher frequencies, signal leakage is seen, and at 40 kHz, about 55 dB of range is available.

If the input is left without a shunt resistor, the leakage through the capacitance of the "Calibrate" switch is the limiting factor at 200 Hz and above. At 20 to 40 kHz, this signal is within 20 dB of a direct connection. A more elaborate switch arrangement would avoid this problem. However, for most transmission applications the measurement port will be either driven by a low impedance, or can be terminated by 50 Ω, removing the issue.

In summary, the ADCs on the audio adapter board are extremely linear. The DSP-based *I-Q* mixers and the associated sine and cosine generators are very accurate. This results in amplitude and phase measurements that do not limit the impedance or transmission measurements, except when the levels are 60 or 70 dB down, which is low enough to make noise a factor. For impedance measurements, this puts the limitations on the analog circuitry. Here uncertainty of the reference resistors is limiting for the middle range of resistance and reactance values, perhaps for 1 to 100 kΩ. Outside this range noise and ADC resolution become issues, but still allow useful measurements from about 0.1 Ω to 1.0 MΩ. Transmission measurements, for most applications, are limited only by the noise floor.

Applications

The real fun of a project like this is performing measurements. Here are the steps to make these measurements in 1-2-3 fashion.

1 — Apply the 5 V, and a greeting screen appears.

2 — Touch "Set Ref R" and select "5K". Touch "Back".

3 — Touch "Single Freq" a frequency selection screen appears.

4 — Touch "Freq Up" until "Freq = 2,000 Hz" appears.

5 — Connect the component to the terminals, in our case a 0.02 μF capacitor.

6 — Touch "Meas Z" causing an automatic calibration and measurement.

7 — The screen of Figure 7 shows a series measurement of 20.01 nF (0.02001 μF) with a *Q* of 1845.9.

There is more data on the screen. It shows a series resistance of 2.155 Ω, and also component values that are marked "Par" for parallel. This means that at 2,000 Hz, the effect of a 7.342 MΩ resistor in parallel with our capacitor is indistinguishable from the series 2.155 Ω value. Both answers are correct. For lower *Q* capacitors (or inductors) the capacity value will be different for the parallel model than it is for the series model, see the sidebar, "Series and Parallel Components". The number of digits of resolution should not be used as an indicator of accuracy. However, there are instances where the extra resolution is useful for observing differences of components.

Let's design an *LC* audio filter using an old inductor component as a basis. The 88 mH toroidal inductors were used in huge quantities by telephone companies. Ray Cannon, W7GLF, gave me a few for this design. Step 1: characterize the inductor. Impedance measurements were made with the 50 and 5 kΩ reference resistors. At the frequency extremes, which are also the impedance extremes, the measured results differed. In the central region from around 100 to 5,000 Hz, the results were very similar. The final data was selected by using the 50 Ω reference for impedances below about 500 Ω (up to 500 Hz) and the 5 kΩ reference data for the higher impedance levels (above 500 Hz). Figure 8 shows the measured inductance and *Q*. The inductance for lower frequencies was about 84.5 mH. The rising inductance at the higher frequencies is a normal result of the inductance approaching its parallel resonant point. The *Q* has a distinct peak around 5,000 Hz, as is normal. In the audio range, the *Q* is lower, but adequate for filter design.

A top coupled filter[14] was designed as shown in Figure 9. This design includes small alterations to use available capacitors that were measured with the AVNA. The *ARRL Radio Designer* program was used to predict the network behavior. Instead of describing the toroids by a single inductance and *Q*, the 88 mH toroid was entered as a table of measured impedances, converted to reflection coefficients.

The filter was built up with free-form construction and tested between 50 Ω terminations using the AVNA "Transmission" function. Figure 10 shows both the predicted and measured insertion loss and insertion phase. The exact response is not the feature to look for, but rather the differences between the predicted and measured values. This is one validation of the full AVNA accuracy, as it is built on the ability to measure both the component impedances and the transmission amplitude and phase. The curves show very tight agreement below 950 Hz and adequate agreement above that frequency. The largest

Series and Parallel Components

The AVNA displays impedances in two forms, a series resistance and reactance, as well as a parallel resistance and reactance. The reactance can represent either an inductance or a capacitance. Any impedance can be represented as either a series or as a parallel combination. Measured externally, they are indistinguishable.

For some purposes, it is easiest to think of the inductor and resistor in series. Actually, resistance is distributed through the inductor, so neither model is precise physically. A contrasting example is a resistor that has a parallel capacitance. For this case, the series resistance and capacitance is valid, but not generally as useful as the parallel model.

What may be surprising at first glance is that the component values depend on whether they are considered in series or parallel. By example, suppose we have an inductor at a frequency where the series reactance X_s is 100 Ω. Furthermore, let the *Q* be 5 so that the series resistance R_s is 100/5 or 20 Ω. In complex arithmetic, the series connection for the impedance *Z* is:

$Z = 20 + j\,100$.

For the parallel model, we first need to find the admittance that is the inverse of the impedance. In our example, the admittance *Y* is:

$Y = 1/Z = 1 / (20 + j\,100)$

After some manipulation we find:

$Y = (20/10400) - j\,(100/10400)$.

From this form we can get the parallel component conductance and susceptance that we are looking for by inverting real part of *Y*, the conductance, to get the equivalent parallel resistance:

$R_p = 10400/20 = 520\ \Omega$,

and taking the imaginary part of $1/(-j\,(100/10400))$, the susceptance, to get the equivalent parallel reactance:

$X_p = 10400/(100) = 104\ \Omega$.

The series resistance was 20 Ω, and the parallel resistance is 520 Ω. [Notice that $Q = X_s/R_s = R_p/X_p = 5$ remains invariant.— *Ed.*]. Perhaps surprising is that the apparent inductive reactance has changed from 100 to 104 Ω. As noted, this shift in apparent inductance diminishes as the *Q* increases. The AVNA displays theses values using this same arithmetic.

discrepancy is the predicted loss (dashed) at 1,000 Hz, 0.75 dB less than that measured (solid). Speculation is that errors in inductor *Q* measurement may be a factor here, as high-*Q* values can be difficult to measure.

Another application is the measurement of the active phase shift network for a direct conversion receiver. In addition to use as a design aid, this could have value in troubleshooting an *I-Q* receiver or transmitter. The circuit tested was a mini-R2 receiver[15] designed by Richard Campbell, KK7B. The portion of the circuitry is from the mixer output, where audio first appears through the filtering and active phase shift networks. The circuit operates with two cascaded all-pass networks arranged so that the difference between the two paths is close to 90° throughout the voice audio band.

For a simple experiment, the *I* and *Q* channels were measure in the transmission mode, doing a sweep over the standard 13 frequencies between 10 Hz and 40 kHz. The 13 frequencies are not enough to show all

DSP Code in the Teensy Arduino

A collection of DSP-specific instructions are built into the ARM Cortex-M4 processor used in the Teensy 3.6. Accessing these can be tedious as many details involved. PJRC, with help from users, has produced an Arduino Audio software library that hides everything not normally used. This is all open software, and can be altered if needed.

Along with the library, there is a drag-and-drop graphical design tool to control the structure of the DSP processing. A simplified version of the measurement channel for the AVNA, as produced by the design tool, is in Figure 13.

The names are assigned automatically, and need translation into AVNA terms. For instance, "waveform 1" is the sine wave generator and "waveform 2" is the sine wave generator shifted 90° (a cosine wave). The "queue" blocks transfer data from the time critical DSP processing to the conventional processing. The i2s1 output is the DAC.

Part of this same design tool is a code generator that created the code in Table A. The names, such as AudioInputI2S (the ADC converter), are C++ objects that are part of the library. Names such as "audioInput" are instances of these objects, and as can be seen, there can be many instances for any object. The "AudioConnection" objects appear as connecting lines in the design tool. They do much more than a simple line would suggest. They control the order that computations will occur, thus they make sure that delays are provided as needed. In addition, for efficiency reasons, all of this DSP is done in blocks, typically 128 long. This requires memory arrays to store data at various points, and this storage is allocated automatically.

In practice, very few lines of the Arduino sketch (program) are used for DSP. A 1,000 Hz sine wave generator is created by the code in Table B. It will compute sine waves at the chosen sample rate until changed. Follow on steps, such as the multipliers, require no instructions once they have their instances declared.

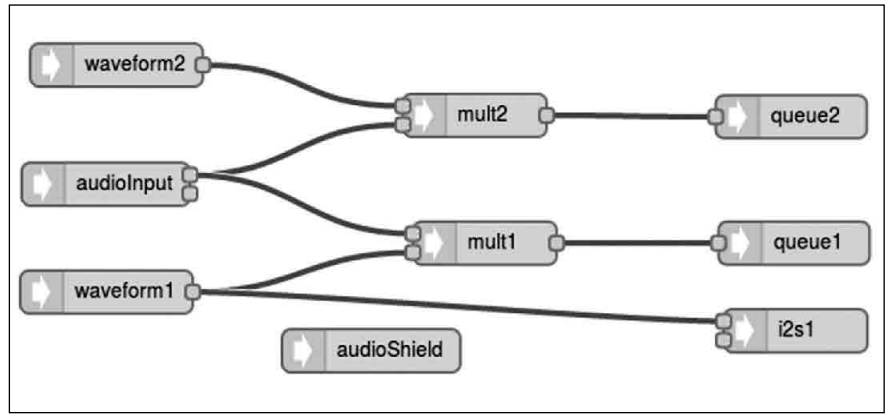

Figure 13 — The graphical DSP description produced by the PJRC design tool.

Table A. DSP Code for describing the block diagram of Figure 13.

```
// GUItool: begin automatically generated code
AudioInputI2S            audioInput;                    //xy=76.5,247
AudioSynthWaveform       waveform1;                     //xy=77,322
AudioSynthWaveform       waveform2;                     //xy=84,164
AudioEffectMultiply      mult2;                         //xy=333,199
AudioEffectMultiply      mult1;                         //xy=340,288
AudioRecordQueue         queue2;                        //xy=553,200
AudioRecordQueue         queue1;                        //xy=555,288
AudioOutputI2S           i2s1;                          //xy=556,349
AudioConnection          patchCord1(audioInput, 0, mult2, 1);
AudioConnection          patchCord2(audioInput, 0, mult1, 0);
AudioConnection          patchCord3(waveform1, 0, mult1, 1);
AudioConnection          patchCord4(waveform1, 0, i2s1, 0);
AudioConnection          patchCord5(waveform2, 0, mult2, 0);
AudioConnection          patchCord6(mult2, queue2);
AudioConnection          patchCord7(mult1, queue1);
AudioControlSGTL5,000    audioShield; //xy=261,363
// GUItool: end automatically generated code
```

Table B. for generating a 1000 Hz sine wave.

```
waveform1.begin(WAVEFORM_SINE);
waveform1.frequency(1,000.0);
waveform1.amplitude(1.0);
waveform1.phase(0.0);
```

Table C. for finding RMS amplitude.

```
amplitudeMeas = sqrt(aveIm * aveIm + aveQm * aveQm);
```

Non-standard computations, such as finding the amplitude of each channels is done by operating on the integer data from queue1 and queue2. This can be operated on as integers, floating point variables, or double precision floating point, as required. For instance the amplitude is found from the averages of *I* and *Q* by the code line in Table C, where in this case all variables are double precision. As can be seen, the DSP code writing has been made very accessible.

the subtle detail but it is quite adequate for trouble-shooting. 500, 1,000 and 2,000 Hz are well inside the design phase-shift region and 200 Hz is close to the region. The measurement needed to allow for the 40 dB gain of the amplifier that precedes the phase shift networks. A 50 Ω attenuator was placed at the two parallel connected mixer outputs in the Mini-R2. The mixers had no LO connection and so as far as affecting the 10 mV level signals, they didn't exist.

Before connecting the signal source to the attenuator, the AVNA was set to transmission measurements using the 50 Ω source resistor. This was done over the serial control line so that the output data could be retrieved directly to the PC. Data plotting was done with a *Gnumeric* spread sheet program. Calibration was also under PC control, which is simple since the 13 frequencies are calibrated as a group. Following calibration, swept transmission measurements were made for both channels of the receiver and taken from the serial terminal in the PC.

Omitting the various steps to process the data in the spread sheet, the difference in the phase shifts of the *I* and *Q* channels was calculated by taking the difference in the phase measurements. Figure 11 shows the results. The three in-band frequencies are within 0.7° of the ideal 90°, constituting a vote of confidence for both the receiver and the AVNA! Not shown is the ratio of amplitude measurements for *I* and *Q*, but all three in-band frequencies had ratios within 0.1 dB. Most of this is correctable with the trimmer pot leaving an uncorrected ratio of only 0.03 dB.

Under PC control, the AVNA can measure at any number of frequencies, not just the stored 13. For circuits such as these phase shift networks it could be useful to place 50 or more data points in the 200 to 5,000 Hz range. When using serial control, there is also provision for uncorrected measurements, meaning that all calibration can be done in the PC control program. This is convenient as it allows all calibration to be done first, and then any number of measurements later, the same as is done in the AVNA for the simple sweep.

Finally, the "What?" function is shown in Figure 12 with a 50 μH inductor measuring 49.24 μH.

Summary and Acknowledgment

This project provides high accuracy impedance and transmission measurements throughout the audio frequency range. It can be used either as a standalone measurement instrument or under PC control as a controllable measuring head. The analog portion of the project is on a home-built printed circuit board. The Teensy 3.6 board, audio CODEC adapter, and Touch Display can all be purchased assembled.

For impedance measurements, the approximate range for highest accuracy is impedance levels from 5 to 50 kΩ. With a frequency range of 10 to 40,000 Hz, this covers resistors from 5 to 50 kΩ, inductors from 20 μH to 800 H, and capacitors from 80 pF to 3,000 μF.

Measurements of a tenth to ten times these values are reliable and of good quality. Beyond that point, some measurements are still quite useful. In particular, capacitors less than 8 pF can be measured at 40 kHz by observing the residual capacity with no component attached, and subtracting that value. Transmission measurements of gain and loss cover a 50 to 70 dB dynamic range, and include both amplitude and phase.

Major credit goes to Paul Stoffregen at PJRC and the many contributors to the Teensy family of boards and software. In addition, this project benefited from hardware, ideas and reviews by Russ Carpenter, AA7QU; Johan Forrer, KC7WW; Jimmy Oldaker, W7CQ; Larry Liljequist, W7SZ; Ray Cannon, W7GLF; and Mike Reed, KD7TS.

Bob Larkin, W7PUA, has been active in Amateur Radio since he was first licensed in 1951 as WN7PUA. He received a BSEE from the University of Washington and an MSEE from New York University. He is retired from a career in electronic circuit and system design along with work in analog and digital signal processing. He continues an interest in Amateur Radio applications in these areas, as well as boat building and sailing.

Notes

[1]Information on the N2PK 50 kHz to 60 MHz VNA, **n2pk.com/#TP1**.

[2]T. C. Baier, DG8SAQ, "A Low Budget Vector Network Analyzer for AF to UHF," *QEX* Mar./Apr. 2007, pp. 46-54; and, "A Small, Simple, USB-Powered Vector Network Analyzer Covering 1 kHz to 1.3 GHz," *QEX* Jan./Feb. 2009, pp. 32-36.

[3]G. R. Steber, WB9LVI, "A Low Cost Automatic Impedance Bridge," *QST* Oct. 2005, pp. 36-39; and, "LMS Impedance Bridge," *QEX*, Sep./Oct. 2005, pp. 41-47.

[4]J. Audet, VE2AZX, "A Low Frequency Adapter for your Vector Network Analyzer," *QEX* Jan./Feb. 2015, pp. 10-16.

[5]See **https://www.pjrc.com/store/teensy36.html**.

[6]See **https://www.pjrc.com/store/display_ili9341_touch.html**.

[7]PCB is available in KiCad format. Boards can be ordered in multiples of 3 from OSH Park company, **https://www.oshpark.com/shared_projects/BjMLw9B9**.

[8]All project hardware and software files are open source and available from **www.arrl.org/qexfiles**. For additional information see **www.janbob.com/electron/AVNA1/AVNA1.htm**.

[9]See **https://www.arduino.cc/en/Main/Software** for Arduino Integrated Development Environment (IDE) that can be extended to handle the Teensy boards.

[10]See **https://www.pjrc.com/teensy/teensyduino.html** for extensions to use with the Arduino IDE.

[11]See **n2pk.com/VNA/RFIV_Single_%20Detector_Switch_%20and_%20Sensors_V1c.pdf**.

[12]See **https://www.pjrc.com/store/teensy3_audio.html**.

[13]See **https://www.arduino.cc/en/main/arduinoBoardUno**.

[14]Designing double-tuned LC filters, Section 3.3 in W. Hayward, W7ZOI, R. Campbell, KK7B and R. Larkin, W7PUA, *Experimental Methods in RF Design*, ARRL publication No. 9239, available from your local ARRL dealer or from the ARRL Bookstore. Telephone toll free in the US:888-277-5289 or call 860-594-0355, fax 860-594-0303; **www.arrl.org/shop**; **pub-sales@arrl.org**.

[15]The Mini-R2 receiver by KK7B, Section 9.9, *Experimental Methods in RF Design,* op. cit.

Ulrich L. Rohde, N1UL and **Ajay K. Poddar, AC2KG**

990 Cape Marco Drive Merida, Penthouse 2,
Marco Island, FL 34145; **ka2weu@aol.com**

2 River Drive, Elmwood, NJ 07407-1828;
akpoddar@synergymwave.com

An Optimized Grounded Base Oscillator Design for VHF/UHF

Phase noise in oscillators, along with frequency stability and efficiency, is an important parameter in oscillator design.

The design of VHF/UHF oscillators has been described in many books and journals with most of the emphasis on frequency stability and to some smaller part on output/efficiency. Since the introduction of reliable phase noise measurements and the ability to predict/simulate the phase noise, the improvement of this important parameter with the help of CAD and analytic equations has gained more attention. The vast majority of early publications focused on designs using small signal approaches, which give non-reliable answers for output frequency, output power and phase noise. The purpose of this paper is to validate the large signal time domain approach using the grounded base oscillator rather than the Colpitts oscillator. The key contributions are: (1) to predict the phase noise correctly using the large signal time domain calculations (Bessel functions) and nonlinear CAD simulators and derive a set of algebraic equations for the noise calculations (many of the CAD tools give incorrect answers about the phase noise), and (2) to provide a set of empirical equations to guide the synthesis of such "optimized" oscillators. This novel design concept using a time domain approach provides both the best output power and the best phase noise.

To have a point of reference the traditional small signal approach is first used followed by the novel approach shown here to get the optimum design. Using a mix of linear equations and one large signal parameter (g_m), the important noise parameters are calculated and validated. Finally, based on this, a very simple but powerfully scalable set of formulas for the oscillator synthesis is shown, that provides extremely good results. In addition to this, the design principle for fixed or narrowband oscillator discussed here also applies to the broadband VCO design. We have shown that this design methodology works over a multi-octave tuning range.

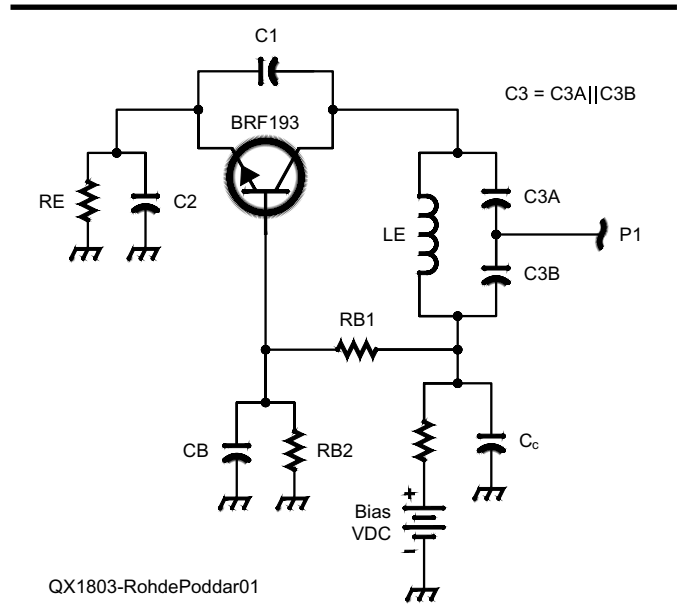

Figure 1 — Typical configuration of grounded base oscillator circuit.

Reference Circuit

A very popular circuit for VHF/UHF oscillators is the grounded base configuration, which is shown in Figure 1. Its phase noise can be made very good, since the RF voltage swing at the collector can be close to the supply voltage. The circuit is simple and has been used for decades. The oscillator function is based on the principle that power from the output is taken and fed to the emitter. This feedback arrangement generates a negative resistance at the output, compensating the losses of the output-tuned circuit, and starts oscillating and then stabilizing the oscillation amplitude[1 – 4]. A complete survey[5 – 19] of configurations and applications is referenced in the Notes. The design methodology works over a 3:1 frequency tuning range[20-23].

Several books on the topic of oscillators have been published in the recent years, and the most popular ones are listed in the Notes. Many of the authors have attempted to predict the oscillator's performance based on a set of linear calculation including using the Leeson model [See Leeson[24]. — *Ed.*] or similar methods to determine the phase noise[25,26]. The problem is that there are important input parameters required, such as the large signal noise figure of the transistor, output power and operating Q. These are typically guessed, but not known. The first successful attempt to determine the large signal phase noise was by Rizzoli, et al.[6] and Annzil, et al.[7].

But these approaches were not useful without a CAD tool and don't give any design guides. Another interesting phenomenon that

has been overlooked by the linear approach is that prediction of the exact oscillator frequency that can be far off compared to the actual frequency of oscillation.

The recent book by Gonzalez[8] gives an interesting overview of designing oscillators using linear calculations and CAD, but his design does not provide the optimum solution. To demonstrate this we are going to first use his way to design a 144 MHz Oscillator. The resulting circuit neither gives the best output power nor the best phase noise and, at high frequencies, requires values for the capacitors, which cannot be easily realized because of parasitic effects. Figure 1 shows the typical configuration of the grounded base oscillator circuit.

This oscillator type works well from RF frequencies like 10 MHz to above 1000 MHz. We will now follow the method of Gonzalez. For large signal conditions see Clarke[11]. Kenneth Clarke was probably the first to publish the effect of the collector current conducting angle of an oscillator, but makes no mentioning of the relationship of it on the phase noise, which is done by Johnson[10].

The [*Y*] parameters

The first step is to determine the small signal [*Y*] parameters for the transistor BFR 193 (Infineon), at the frequency of 144MHz, and the operating point: I_c = 10 mA, I_B = 24 µA, V_{be} = 0.64V, V_{ce} = 8.8 V

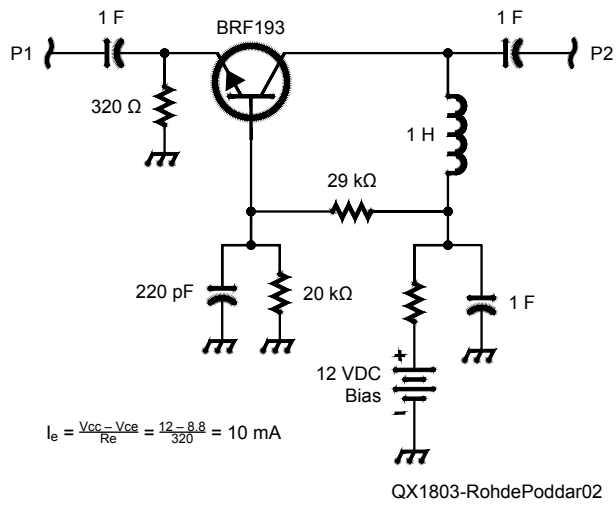

Figure 2 — Small signal *Y* parameter generating circuit with CAD using Infineon time domain model

The 10 mA operating point was selected for a stable transistor cut-off frequency f_T. For more output power 30 mA is a better choice.

Figure 2 shows the circuit generating the small signal [*Y*] parameters using the Ansoft Designer CAD and the time domain model.

The CAD software generates the *Y*-parameters based on the following definition in Figure 3(a).

$$\begin{bmatrix} I_1 \\ I_2 \end{bmatrix} = \begin{bmatrix} Y_{11} & Y_{12} \\ Y_{21} & Y_{22} \end{bmatrix} \begin{bmatrix} V_1 \\ V_2 \end{bmatrix}$$

We obtain:

$$Y_{11} = G_{11} + jB_{11} = (279.08 - j95.07) \text{ mS}$$
$$Y_{21} = G_{21} + jB_{21} = (-271.32 + j100.77) \text{ mS}$$
$$Y_{12} = G_{12} + jB_{12} = (-1030 + j78.06) \ \mu\text{S}$$
$$Y_{22} = G_{22} + jB_{22} = (1020 + j536.14) \ \mu\text{S}$$

Parallel Feedback Oscillator Topology

The feedback arrangement shown in Figure 3(b) is the standard feedback Oscillator topology using parallel elements. Theoretically the grounded base configuration can be rotated to be the Colpitts circuit. This statement is often found in the literature, see Kotzebue and Parrish[5]. It is based on the black box theory. If we look at the performance, it is not correct that a mathematical rotation yields the same performance. In the case of the Colpitts Oscillator the RF voltage swing is now limited by the base emitter and emitter to ground voltage and as a result there is less energy stored in the circuit and because of loading the operational *Q* can be less than in the grounded base configuration. Here V_{cb} is about 12 V. Also Y_{22cb} is less than Y_{22ce}, resulting less loading. The Colpitts oscillator is popular because of its simplicity, and its perceived high isolation as the output power is taken at the collector. However, due to the strong Miller effect at very high frequencies, this is not a true statement. These comments set aside the general approach in the time domain shown here is valid not only for the Colpitts Oscillator but other derivatives.

The necessary oscillation condition for the parallel feedback oscillators as shown in Figure 3(b) can be described by

$$Y_{out} + Y_3 \Rightarrow 0$$

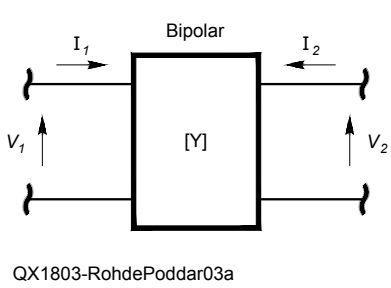

Figure 3(a) — *Y*-parameters based this definition.

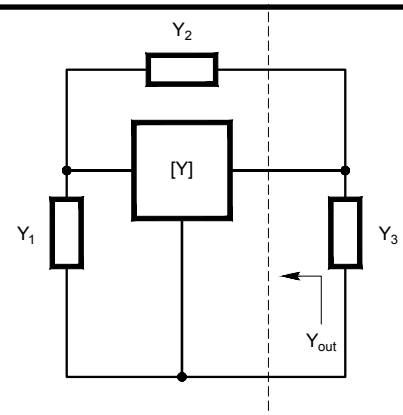

Figure 3(b) — Parallel feedback oscillator topology.

This condition can be expressed as

$$Det\begin{bmatrix} Y_{11}+Y_1+Y_2 & Y_{12}-Y_2 \\ Y_{21}-Y_2 & Y_{22}+Y_2+Y_3 \end{bmatrix}=0$$

$$Y_3=-[Y_{22}+Y_2]+\frac{[Y_{12}-Y_2][Y_{21}-Y_2]}{[Y_{11}+Y_1+Y_2]}$$

where Y_{ij} $(i, j = 1, 2)$ are the small signal $[Y]$ parameters of the bipolar or FET model.

Calculation of the feedback network values [linear case]

As shown in Figure 3(b), the active 2-port network, together with the feedback elements Y_1 and Y_2, are considered as a one-port negative resistance oscillator circuit. The following is an example of an oscillator design using the small signal parameter determined above at 8.8 V and 10 mA at 144 MHz. The output admittance Y_{out} is

$$Y_{out}=-Y_3$$

$$\Rightarrow[Y_{22}+Y_2]-\frac{[Y_{12}-Y_2][Y_{21}-Y_2]}{[Y_{11}+Y_1+Y_2]}$$

The optimum values of feedback element are calculated from the expression of B_1^* and B_2^*, and for 10 mA are:

$$B_1^*=-\left\{\begin{array}{l} B_{11}+\left[\dfrac{B_{12}+B_{21}}{2}\right] \\ +\left[\dfrac{G_{21}-G_{12}}{B_{21}-B_{12}}\right]\left[\dfrac{G_{12}+G_{21}}{2}+G_{11}\right] \end{array}\right\}$$

$$jB_1^*=j\omega C_1$$

$$C_1\cong 478\,pF$$

$$B_2^*\cong 417\times10^{-3}$$

$$jB_2^*=j\omega C_2$$

$$C_2\cong 459\,pF$$

The optimum values of the real and imaginary part of the output admittance are

$$Y_{out}^*=[G_{out}^*+jB_{out}^*]$$

where

G_{out}^* and B_{out}^* are values for conjugate matching.

$$G_{out}^*=G_{22}-\left[\frac{(G_{12}+G_{21})^2+(B_{21}-B_{12})^2}{4G_{11}}\right]$$

$$\approx -74.5\times10^{-3}$$

needed to compensate the resonator losses ,

$$B_{out}^*=B_{22}+\left[\frac{G_{21}-G_{12}}{B_{21}-B_{12}}\right]\left[\frac{(G_{12}+G_{21})}{2}+G_{22}-G_{out}^*\right]+\left[\frac{B_{21}+B_{12}}{2}\right]$$

$$\approx 214.74\times10^{-3}$$

$$C_3\approx 237\,\text{pF}$$

$$\omega_0=\frac{1}{2\pi\sqrt{LC}};\quad C\approx 471\text{ pF}$$

For $f_0=144$ MHz, $L_3\approx 2.59$ nH

Figure 4 shows the 144MHz oscillator circuit using the small signal Y parameter for establishing oscillation conditions. The required values for this parallel feedback topology are: 478 pF for the feedback capacitor, 459 pF for the emitter to ground, the inductor 3.2 nH, and 186 pF for C_{3A} and C_{3B}. The bypass capacitors C_b and C_c should be about 220 pF.

However, it is practically impossible to manufacture capacitors above 200 pF to be capacitive at these frequencies. The best but awkward method then is to use a few capacitors in parallel.

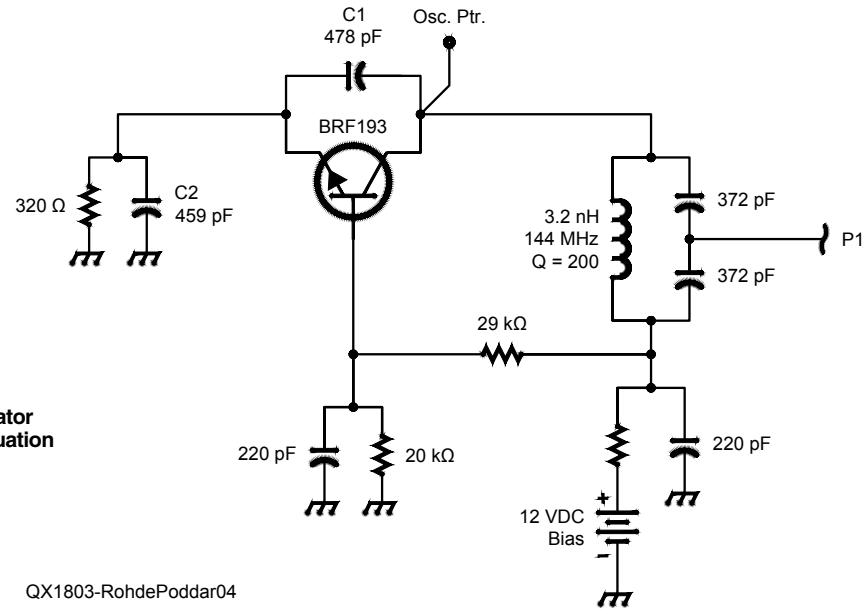

Figure 4 — 144 MHz oscillator reference circuit for the evaluation of the linear approach.

QX1803-RohdePoddar04

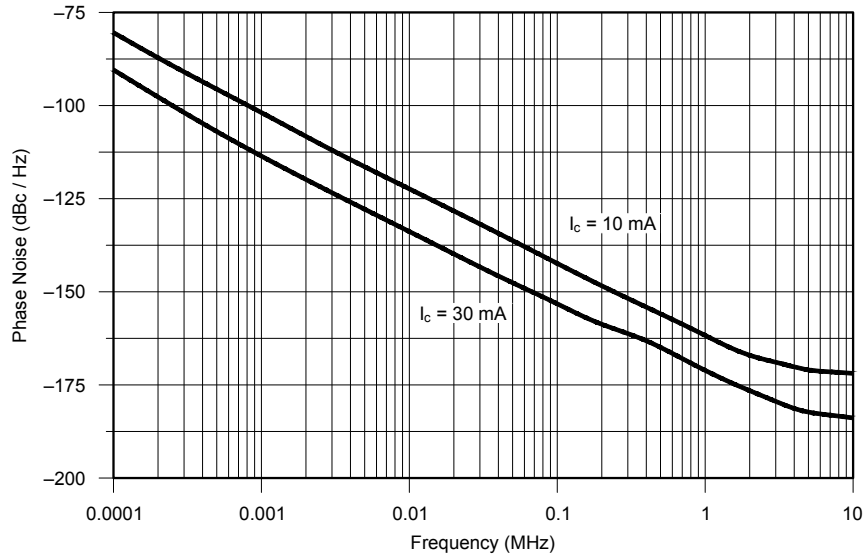

Figure 5 — Phase noise plot of 144 MHz oscillator reference circuit for the evaluation of the linear approach (both 10 mA and 30 mA cases). The 30 mA case gives 10 dB lower phase noise than the 10 mA case.

For 30 mA,

$$Y_{11} = G_{11} + jB_{11} = (437 - j295)\ \text{mS}$$

$$Y_{21} = G_{21} + jB_{21} = (-427 + j296)\ \text{mS}$$

$$Y_{12} = G_{12} + jB_{12} = (-1670 + j757)\ \ \mu\text{S}$$

$$Y_{22} = G_{22} + jB_{22} = (1650 - j146)\ \ \mu\text{S}$$

For f_0 = 144 MHz and 30 mA, the component values are L = 3.77 nH, C_1 = 518 pF, C_2 = 503 pF, C_3 = 69 pF, C = 324 pF, needless to say C_1 and C_2 are paralleled capacitors in the vicinity of 100 pF each.

Figure 5 shows the simulated plot of the phase noise. The "linear "calculation indicates a resonant frequency of 143.2 MHz, while the non-linear harmonic balance (HB) analysis supplies the correct frequency of 144.2 MHz (quite a difference in percent) and an output power of just 5.1 dBm, as seen in Figure 6. This value is determined using the HB programs Ansoft Designer (Nexxim). ADS gives the same answer. These CAD tools deviate less then 1 dB from measured results, if the input Spice type parameters for the transistor are accurate.

Large signal and noise analysis

There were a variety of efforts made to deal with the large signal conditions, like the time domain approach. Equation (10) in Johnson[10] is a first successful attempt to deal with the calculations of the output power with reasonable effort. There are many problems associated with both the large signal analysis as well as the noise analysis. From an experimental point of view it is virtually impossible to build all possible variations. So we were trying to determine if the Ansoft Designer, whose large signal noise analysis development we were involved with, would give us the correct prediction. We were aware that all researchers would primarily look for measured data (which we will show) and yet we had to convince them that our CAD tool

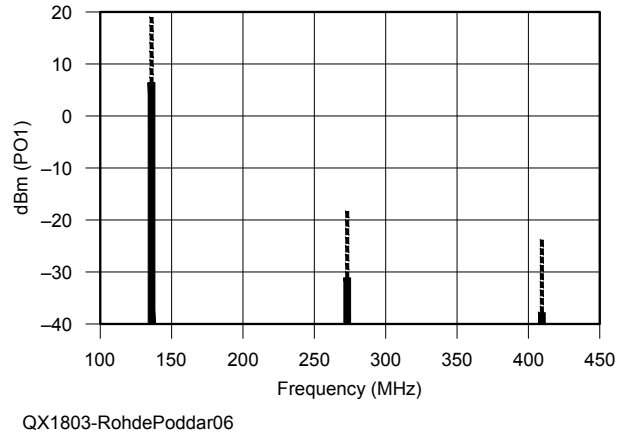

Figure 6 — RF output power of 144 MHz oscillator reference circuit for the evaluation of the linear approach Both 10 mA (solid) and 30 mA (dashed) are shown. For 30 mA, 12dB more power is available, now a total of approximately 18 dBm.

was reliable. Therefore we took a few critical circuits, running from crystal oscillators to VCOs and evaluated them again. These were available during the development of the Designer CAD tool, and we re-measured them, with more refined test equipment like the R&S FSUP 26 and its necessary options. We have shown[12, 13] that the accuracy of the prediction was within 0.5 dB of the measured results. During this effort to analyze the noise in oscillators with a set of equations using a minimum of expensive CAD tools, we found this was possible. These equations[9] will be used here.

A Novel Approach using the time-domain analysis for obtaining the best phase noise and output power.

The hunt for a combined low phase noise can be followed through the literature. Designers have published recipes, like the

DX ENGINEERING®

Showroom Staffing Hours:
9 am to 5 pm ET, Monday-Saturday

Ordering (via phone):
8:30 am to midnight ET, Monday-Friday
8:30 am to 5 pm ET, Weekends

Phone or e-mail Tech Support: 330-572-3200
8:30 am to 7 pm ET, Monday-Friday
9:00 am to 5 pm ET, Saturday
All Times Eastern I Country Code: +1
DXEngineering@DXEngineering.com

800-777-0703 | DXEngineering.com

Get Ready for Field Day Fast and for Less with DX Engineering!

New!

DXE-200FD-P

DX ENGINEERING

LBS LOW BAND SYSTEMS

Field Day Triplexer Combo

We've made it easy to work the 20, 15 and 10 meter bands with three different radios, using just a single tri-band antenna! Our Field Day Triplexer Combo includes Low Band Systems' (LBS) innovative 200W Triplexer (LBS-PB-TP200), LBS 20/15/10M band-pass filters, and coaxial cable jumpers. Choose from RG8X cable or high-performance RG400. It's a simple way to get the most out of Field Day. Eliminate the need (and cost) for extra antennas while enjoying fast setup and worry-free operation without RF interference. The system works with any tri-bander antenna, including DX Engineering's reliable Skyhawk. For more details, visit DXEngineering.com.

DXE-200FD-8X-P...$599.99 **DXE-200FD-P...$699.99**

DX ENGINEERING

DXE-UT-KIT4 DXE-UT-KIT-CC1

Coaxial Cable Tool Kits

The Basic Kit is tailored for RG-213 and RG-8 cable with solder type PL-259 connectors. **DXE-UT-KIT3**

The Complete Kit gives you additional tools to work with RG-8/X size cable and solder type PL-59 and Type N connectors. **DXE-UT-KIT4**

The Ultra-Grip 2 Crimp Connector Kit is ideal for installing crimp connectors on RG-8U, 213 and LMR-400 size cable. It also has dies for RG-8X, PowerPole® and ring terminals. **DXE-UT-KIT-CRMP2**

The F-Connector Coax Cable Tool Kit is made for RG-6 cable and includes 25 of DX Engineering's Snap-N-Seal® watertight F-connectors. **DXE-UT-KITF**

The Coaxial Prep Tool Kit for Crimp Connectors prepares 400MAX, 8U, 213U, LMR-400, 8X and LMR-240 size cables for installation using crimp-style PL-259, N Type and BNC connectors. **DXE-UT-KIT-CC1**

REU-AA-30ZERO

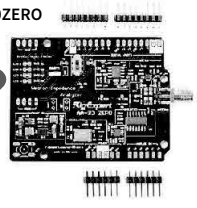

New!

REU-AA-55ZOOM

RigExpert®

Antenna Analyzers and Project Board

Professional broadcasters, telecommunications engineers and serious Amateur Operators all over the planet trust analyzers from RigExpert. They combine functionality, accuracy, durability, and ease-of-use. Maximize your frequency range coverage with the best RigExpert has to offer: the REU-AA-600 (0.1 - 600 MHz), REU-AA-1000 (0.1 - 1,000 MHz), and REU-AA-1,400 (0.1 - 1,400 MHz). For experimenters, RigExpert's 0.06 - 30 MHz Antenna Analyzer Project Board (REU-AA-30ZERO) can be incorporated into a range of products, from making your own automatic antenna tuner to pairing it with the ESP8266 Wi-Fi SoM to remotely perform RF-circuit or antenna analysis. Enter "REU Board Only" at DXEngineering for more details.

DXE-UWA213-KIT

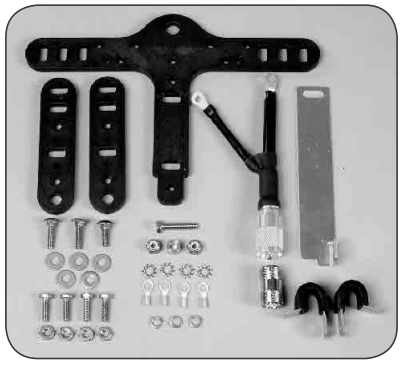

DX ENGINEERING

Wire Antenna Kits

When it comes to portable operation, it's tough to beat the versatility and performance of a wire antenna. DX Engineering has put together EZ-BUILD UWA Center T and End Insulator Kits that let you build virtually any wire antenna type—folded dipole, inverted-vee, off-center fed, Windom, Zepp, loops and more. Multi-band operation is also possible. Search keyword EZ-BUILD at DXEngineering.com to see your options.

YAESU ICOM KENWOOD ALINCO

Free Standard Shipping for Orders Over $99*: If your order, before tax, is over 99 bucks, then you won't spend a dime on shipping. (Additional special handling fees may be incurred for Hazardous Materials, Truck Freight, International Orders, Next Day Air, Oversize Shipments, etc.).

FAST FREE SHIPPING over $99*

Email Support 24/7/365 at DXEngineering@DXEngineering.com ***Stay connected:*** YouTube

use of low noise transistors, high Q circuit, and other things, but the consequences of the large signal operation and the resulting phase noise had not been fully understood. A complete mathematical treatment follows for a 144 MHz oscillator.

Design steps

Step 1 — Calculation of the output power for the selected dc operating conditions.

We select the same circuit as above, and set f_o = 144 MHz.

The RF output current is:

$$\begin{aligned} I_{RF}(t) &= I_c(t) \cong I_e(t) \\ &= I_{dc}\left[1+2\sum_{1}^{\infty}\frac{I_n(x)}{I_0(x)}\cos(n\omega t)\right] \\ &= 10\times10^{-3}[1+6.6]_{x=15} \\ &\Rightarrow I_{RF}(t) = 60 \text{ mA peak amplitude} \end{aligned}$$

where x is normalized drive level

$$x = \frac{qV_1}{kT};\ V_1 = \text{Drive signal}$$

Considering 50 Ω load, the RF output power is calculated:

$$\begin{aligned} V_{RF}(f_0) &= I_{RF}\times 50 \\ &= 60\times10^{-3}\times 50 \\ &= 3 \text{ V peak amplitde} \end{aligned}$$

No V_{ce} saturation assumed.

The oscillator output power at 144 MHz is then

$$\begin{aligned} P_{out}(f_0) &= \frac{V_{RF}^2(f_0)}{2R_L} \\ &= \frac{9}{2\times50} = 90 \text{ mW} = 19.5 \text{ dBm} \end{aligned}$$

Step 2 — Calculation of the large signal transconductance for the normalized drive level x = 15

$$\begin{aligned} \cdot Y_{21}\big|_{\text{small signal}} &= \frac{I_{dc}}{kT/q} = \frac{I_{dc}}{V_T} = g_m \\ \Rightarrow g_m &= \frac{3\times10^{-3}}{26 \text{ mV}} \approx 115 \text{ mS} \end{aligned}$$

where k is the Boltzman constant, and T = 298 K.

The large signal transconductance G_m is now

$$\begin{aligned} Y_{21}\big|_{\text{large-signal}} &= G_m(x) = \frac{qI_{dc}}{kTx}\left[\frac{2I_1(x)}{I_0(x)}\right]_{n=1} \\ &= \frac{g_m}{x}\left[\frac{2I_1(x)}{I_0(x)}\right]_{n=1} \\ &\approx 20 \text{ mS (for } x \approx 15) \end{aligned}$$

This assumes an ideal intrinsic transistor. To perform the transition from the intrinsic to extrinsic transistor, we add the parasitics (package effects, lead inductance and bond wires) by correcting the final results for capacitances and inductances. The f_t of the transistor used is high enough so a phase shift correction for g_m is not necessary at this frequencies (VHF).

The value of n can be in the range of n [n_1, n_2], where n_1 is 2 and n_2 is 5 for a drive level x = 15 (low phase noise performance).

Assume n = 5, the values of C_1 and C_2 can be calculated to be

$$\frac{C_2}{C_1+C_2} = \frac{1}{n} \Rightarrow C_2 = \frac{C_1}{n-1}$$

$$C_2 = \frac{C_1}{n-1} = \frac{C_1}{4} \Rightarrow \frac{C_1}{C_2} = 4$$

The ratio of the capacitor C_1 to C_2 is 4.

Step 3 — Calculation of C_1 and C_2.

The value of C_1 is selected for proper loading, therefore

$$\begin{aligned} &XC_1 > Y_{11} \approx C_1 > \frac{Y_{11}}{\omega} \\ &\Rightarrow C_1 > \frac{Y_{21}}{\omega} \cong C_1 \geq \frac{2G_m(x)}{\omega} \\ &\Rightarrow C_1 > \frac{2\times20\times10^{-3}}{2\times\pi\times144\times10^6} \approx 44 \text{ pF} \end{aligned}$$

For C_1/C_2 = 4, $C_2 \cong$ 11 pF.

Step 4 — Calculation of C_3 and C_4.

For optimum phase noise and power output,

$$C_3 \geq 2C_2 \Rightarrow C_3 = 22 \text{ pF},$$

and the capacitive transformer tapping ratio m (C_3/C_4) should be greater than 10, therefore the impedance transformation is greater than 100. For C_3 =22 pF, C_4 is 220 pF.

Step 5 — Calculation of L.

$$\omega_0 = \frac{1}{2\pi\sqrt{LC}};$$

$$C = C_T + C_3;$$

$$C_T = \frac{C_1\times C_2}{C_1+C_2} \Rightarrow C \approx 30 \text{ pF}$$

For f_0 = 144 MHz,

$$L_3 = \frac{1}{(2\pi\times144\times10^6)^2\times29\times10^{-12}} \approx 39 \text{ nH}$$

Step 6 — Calculation of the [L/C] ratio.

The energy stored across the resonator circuit for a given conduction angle and drive level is dependent on the characteristic impedance,

$$Z_0 = \sqrt{\frac{L(\text{nH})}{C(\text{pF})}} = \sqrt{1200}$$

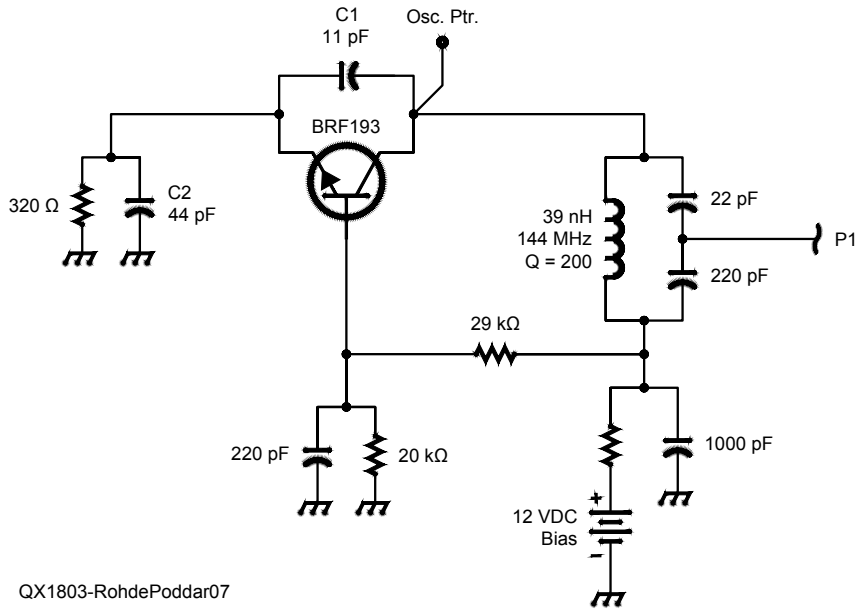

Figure 7 — 144 MHz oscillator reference circuit for the evaluation of the time domain approach.

The total sum of all the four noise sources can be expressed as

$$\begin{aligned} PN(\omega_0+\Delta\omega) &= [PN_{inr}(\omega_0+\omega)] \\ &\quad +[PN_{Vbn}(\omega_0+\omega)] \\ &\quad +[PN_{ibn}(\omega_0+\omega)] \\ &\quad +[PN_{icn}(\omega_0+\omega)] \\ &\cong -94.1\,\text{dBc/Hz} \end{aligned}$$

It appears that the flicker noise and the noise from the resonator are the limiting factors for the overall phase noise performance of the oscillator circuit.

Figure 7 shows the schematic and Figure 8 shows the layout of the 144 MHz oscillator using time domain parameters at I_c = 10 mA. The oscillator circuit shown in Figure 7 uses a lumped inductor of 39 nH and an unloaded Q of 200 at the operating frequency. Even at these frequency the layout is quite critical. The Figure 8 layout shows an assembly of component where the lead inductances have been kept small. The inductor is a standard off the shelf component.

Figures 9 shows the CAD simulated phase noise plot, and Figure 10 shows the measured phase noise plot. The simulated and the validated output power now is 11.55 dBm (a 6 dB improvement compared to the linear case), and at 10 kHz offset from the carrier frequency the phase noise has been improved to be –135 dBc/Hz from previously –122 dBc/Hz, a 13 dB improvement. The outputs at the second and third harmonics are about -28 dBm and -34 dBm.

Using our phase noise calculation approach as shown above, the result is –134 dBc/Hz and –94 dBc/Hz at 10 kHz and 100 Hz offset. All three results, calculated, simulated, and measured result closely agrees within 1 dB. Many designers may not have access to CAD tools with oscillator noise calculation, and therefore this approach is extremely useful and cost saving.

If we now operate the same transistor at 30 mA, the phase noise at 10 kHz offset will be further improved to –144 dBc/Hz and the output power is increased to 20 dBm. This shows that for low phase noise design a more powerful transistor is a good choice. It is important to keep the dc dissipation of the device in mind, as the CAD approach does not flag a misuse of the device.

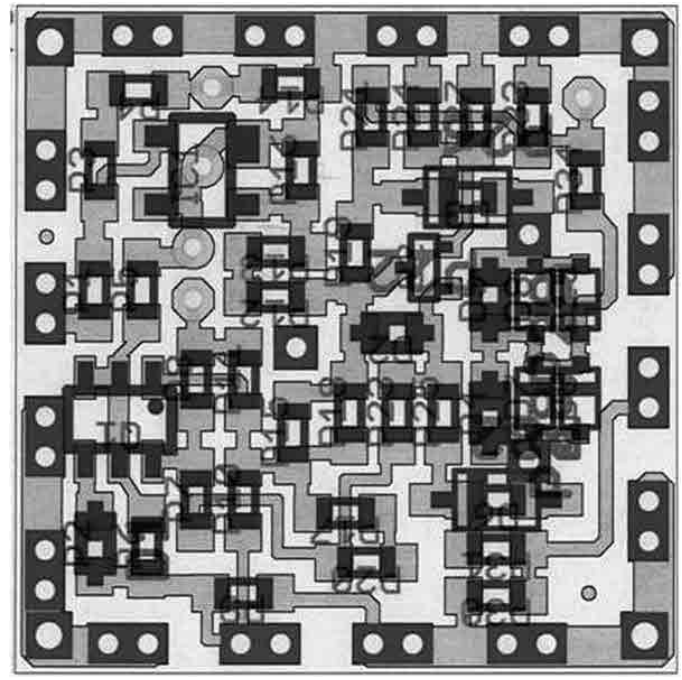

Figure 8 — Layout of 144 MHz oscillator circuit using LC lumped inductor capacitor resonator network

Second Example: 433MHz oscillator circuit

We use the same transistor (BFR193) with, V_{ce} = 8.8V, I_c = 10 mA, I_B = 85 µA, V_{be} = 0.67 V, and we now obtain:

$C_1 = 3.3$ pF, $C_2 = 13$ pF,
$C_{3A} = 7.5$ pF, $C_{3B} = 75$ pF,
$L_E = 13$ nH,
$R_E = 320\ \Omega$, $R_{B1} = 29000\ \Omega$,
$R_{B2} = 20000\ \Omega$,
$C_B = 220$ pF, $C_c = 1000$ pF,
$V_{dc} = 12$ V

resulting an output power of 11.9 dBm and a phase noise of -100 dBc/Hz at 10 kHz offset from the carrier. Since the 144 MHz was about 35 dB better in the phase noise (-135 dBc/Hz at 10 kHz offset), we need to ask why. The phase noise and the carrier frequency are related in a quadratic function. This means three times increase in frequency results in 9 dB degradation in phase noise for 432 MHz oscillator circuit in comparison to 144 MHz oscillator as shown in Figure 7. Therefore, phase noise performance for 432 MHz oscillator circuit should be -126 dBc/Hz instead of -100 dBc/Hz at 10 kHz offset (CAD simulated). The answer is that even in grounded base condition, large signal Re[Y_{22}] loads the parallel tuned circuit significantly resulting in a lower dynamic operating Q. We must find a work around for this.

The phase noise and the Q are related in a quadratic function. This means two times the Q results in 12 dB improvements. Since we lost 26 dB, we need to improve the dynamic loaded operating Q approximately 20 times. As this is not possible, there may be more

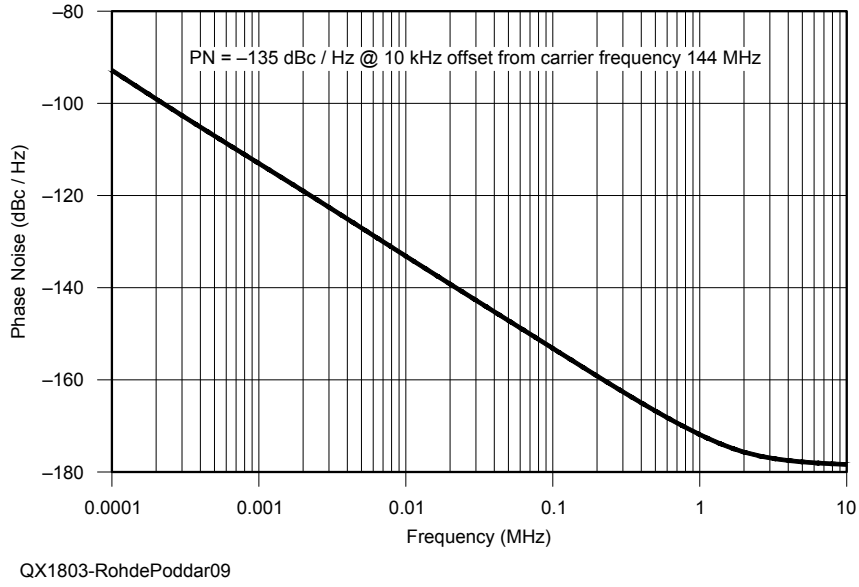

Figure 9 — Phase noise plot of 144 MHz oscillator reference circuit for the evaluation of the time domain approach.

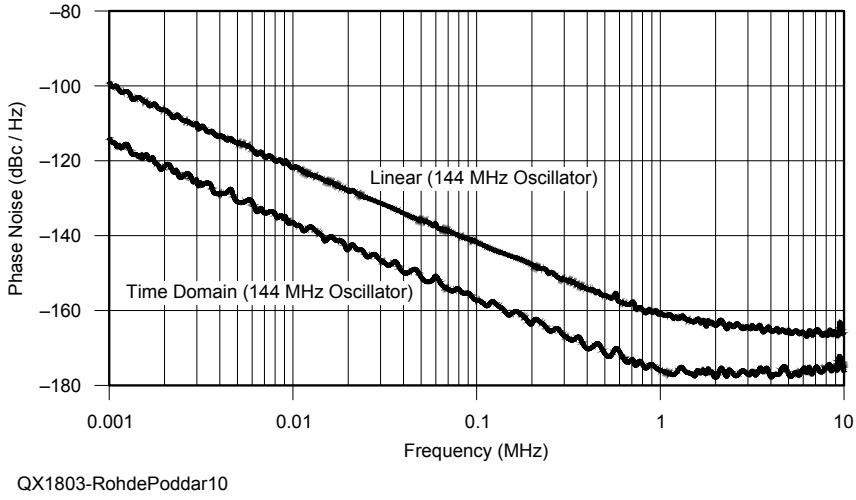

Figure 10 — The measured phase noise plot for 144 MHz oscillator (linear and time domain).

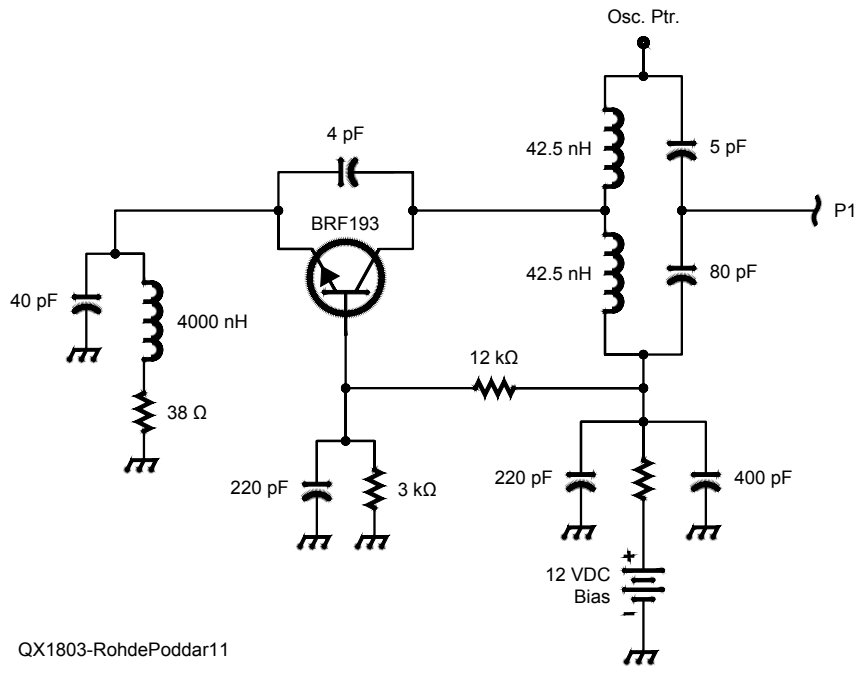

Figure 11 — Schematic of 432 MHz grounded base oscillator using tapped inductor (30 mA).

effects than just the Q deterioration. The answer is, "the collector emitter capacitance dynamically detunes the circuit periodically". A solution for this problem is tapping the inductor, therefore decreasing the influence of the transistor. We will show this now.

Modified Circuit for UHF (432 MHz) and Higher Current

If we inspect Y_{22} of our transistor at 432 MHz and at 30 mA, we will see that the loading of the tank circuit decreases the operating Q significantly. The way around this to apply a center tapped inductor. As the coupling at these frequencies from winding to winding is not extremely high, actually two separate identical inductors can be used successfully.

Figure 11 shows the schematic of a 432 MHz grounded base oscillator using the tapped inductor. This is a modification of the circuit we have used previously. In the case of a VCO, it would be advantageous to use a different output coupling scheme because in this configuration, the loading would vary with frequency. This can easily be achieved by adding some inductive coupling to the circuit. In case of a printed resonator this can be accomplished quite simply.

Figure 12 shows the layout of the 433 MHz oscillator circuit using buried printed coupled line resonator network (stripline resonator: middle layer). The actual resonator would not be visible if the oscillator is visually inspected.

Figure 13 shows the simulated phase noise plot. It shows the expected noise degradation of 9 dB, as the frequency is approximately three times higher. The resulting simulated output power at 432 MHz is 16 dBm, compared to 18 dBm at 144 MHz. This is due to internal package parasitics, which could not be compensated externally. The second harmonic is suppressed by 38 dB; this is due to the higher operating Q.

Circuit Design Guidelines

The results we have obtained so far were based on mathematical calculations. Some of these calculations are difficult to obtain. However, by inspecting the resulting circuits, there are certain relationship between the values of the capacitance of the tuned circuit and the two feedback capacitors, the collector emitter capacitor and the emitter to ground capacitor. The following shows the set of recommended steps for easy design of such oscillator. Figure 14 shows the typical grounded base oscillator for demonstrating the simple design rules where C_E and C_F are the feedback capacitors that

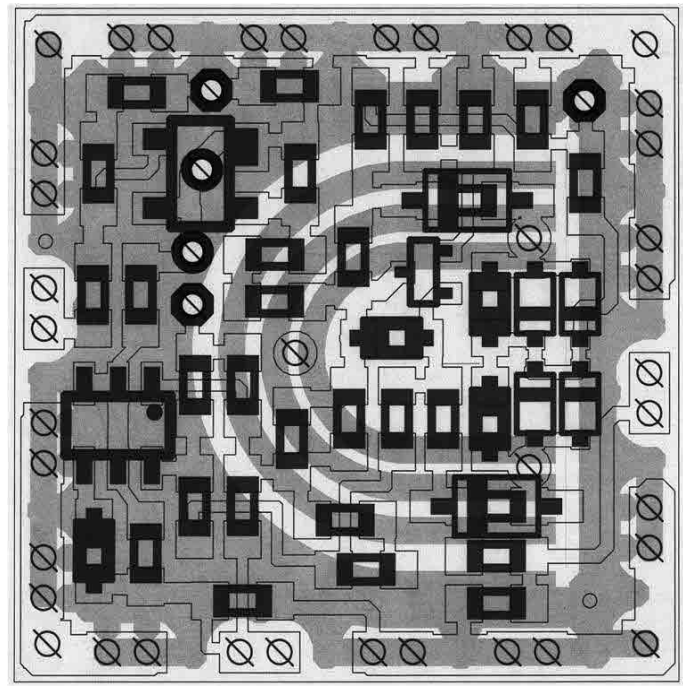

Figure 12 — Layout of the 432 MHz oscillator circuit using buried printed couple line resonator network (stripline resonator in the middle layer).

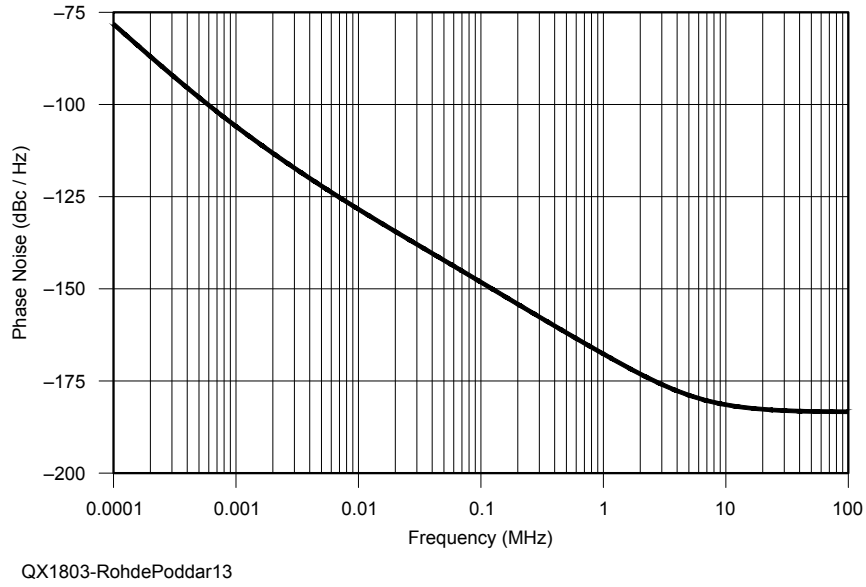

Figure 13 — The simulated phase noise plot of 432 MHz grounded base oscillator using tapped inductors.

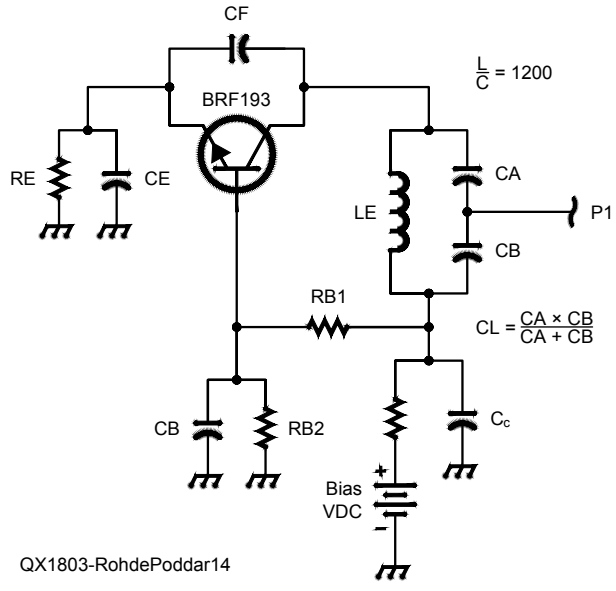

Figure 14 — Typical configuration of grounded base oscillator circuit.

generates the negative resistance to compensates the loss resistance of the resonator network comprised of L_E and C_L^*.

Simple Design Rules With an Example:

By setting the *L/C* ratio to a fixed value of 1200 (this is done for optimum energy storage, group delay and energy transfer for a given cycle in the resonator network), the following should be used.

$$\frac{L}{C} = \left[\frac{L_E}{C_L^*}\right]_{Grounded-Base} = 1200$$

$$\Rightarrow Z_0 = \sqrt{1200} \cong 34.6\ \Omega$$

$$L = 1200 \times C$$

$$\Rightarrow L_E = 1200 \times C_L^*$$

$$f = \frac{1}{2\pi\sqrt{LC}}$$

$$= \frac{1}{2\pi\sqrt{1200}}$$

$$C_L^* = C_L + \frac{C_E C_F}{C_E + C_F}$$

where C_E (C_1) and C_F (C_2) are feedback capacitors.

$$C_L = \frac{C_A C_B}{C_A + C_B};$$

where C_A (C_1) and C_F (C_2) are feedback capacitors.

$C_B = 10\,C_A$.

To examine the accuracy of this simple approach, let us take the same 144 MHz grounded base oscillator as shown in Figure 7.

Example: The 144 MHz Grounded Base Oscillator

$$C_L^* = \frac{1}{2\pi f\sqrt{1200}} \Rightarrow C \cong 31\ \text{pF}$$

$$L_L = \frac{1}{(2\pi f)^2 C} \Rightarrow L \cong 39\ \text{nH}$$

$C_F = 0.3 \times C_L^* \cong 11$ pF

$C_L = 2 \times C_F \cong 22$ pF

$C_E = 4 \times C_F \cong 44$ pF

$C_A = 22$ pF

$C_B = 220$ pF

These results are comparable with the results above and the calculation is frequency scalable with minor corrections possibly, if necessary. Other alternative short formulas based on linear approximations and published in the literature may not deliver the same high performance.

Summary

Today's applications, both commercial and consumer, require low cost high performance oscillators and the design time is also very critical. The approach shown here meets these requirements and gives detailed guidelines for better performing oscillators. The concept is explained in detail and validated. This is only one of the many applications for which this technique is applicable. Furthermore, by translating this design to integrated circuits very high performance but very low cost oscillators can be made. From a theoretical point, we found it surprising that simple equations could be found which optimized the design and accurately predicted the phase noise. For the determination of the output power, a nonlinear CAD tool is recommended if the frequencies are higher than 500 MHz. Our example has shown that at frequencies below 200 MHz the output power can be determined quite accurately using this approach.

To make this oscillator part of a PLL synthesizer, electronic tuning is required. The output capacitor should then have a set of tuning diodes in parallel , with light coupling , to properly select the tuning range.

Prof. Dr.-Ing. habil. Dr. h.c. mult. Ulrich L. Rohde, N1UL, is the Chairman of Synergy Microwave Corp., Paterson, NJ; President of Communications Consulting Corporation, serving as an honorary member of the Senate of the German Joint Forces University Munich; honorary member of the Senate of the Brandenburg University of Technology Cottbus-Senftenberg, Germany; past member of the Board of Directors of Ansoft Corporation, Pittsburgh, PA; and is a partner of Rohde & Schwarz, Munich, Germany. He presented numerous lectures worldwide regarding communications theory and digital frequency synthesizers. Dr. Rohde has published more than 300 scientific papers in professional journals and several books and book chapters, and several dozen patents. Dr. Rohde is a Fellow Member of the IEEE, Member of the IEEE Technical Committee for HF, VHF, and UHF Technology MTT- 17, Member of the IEEE Signal Generation and Frequency Conversion MTT-22, Member of the Board of Trustees Fraunhofer Gesellchaft (EMFT) for Modular Solid State Technology, Member of the Board of Friends of the Bavarian Academy of Science and Humanity, and Honorary Member of the Academy of Science, all in Munich, Eta Kappa Nu Honor Society, Executive Association of the Graduate School of Business Columbia University, NY, the Armed Forces Communications & Electronics Association, Fellow of the Radio Club of America, former Chairman of the Electrical and Computer Engineering Advisory Board at New Jersey Institute of Technology, IFCS C. B. Sawyer Award recipient, IFCS I. I. Rabi Award recipient, Honorary Professor at IIT Delhi, India, Chief Judge of IEEE IMS 2014 Student Design Competition, and PhD Defense Committee Member at UCLA and Drexel University. His hobbies include sailing, US Merchant Marine Officer, Master of Steam or Motor Vessels, photography and licensed Amateur Radio operating since 1956 (DJ2LR and N1UL).

Dr. Ajay Poddar, AC2KG, is an IEEE Fellow, technological leader, and distinguished scientist. He graduated from IIT Delhi, India; Doctorate (Dr.-Ing.) from TU-Berlin, Germany; Post Doctorate (Dr.-Ing. habil) from Brandenburg Technology University, Cottbus, Germany. From 1990 until 2001 he has worked as Senior Scientist and Program Manager at Defense Research & Development Organization (DRDO) India. From 2001, he has been working as a Chief Scientist at Synergy Microwave, responsible for design and development of frequency generating and time keeping electronics, RF-MEMS based microwave/millimeter wave components, Negative Index inspired Metamaterial-Mobius resonators for sensors, and Optoelectronics for industrial, medical, and space applications. Dr. Poddar is a full professor at Oradea University, Romania and Guest lecturer at Technical University, Munich, Germany, and PhD advisor at several universities worldwide. He has received over dozen awards for scientific and technological innovations, over two dozen patents, authored/coauthored 6 technical books, and published over 300 scientific papers in professional journals and conference proceedings. He is a recipient of IEEE 2015 IEEE IFCS W.G. Cady Award, 2015 IEEE R1 Scientific innovation Award, and 2009 IEEE R1 Scientific Contributions Award. Dr. Poddar has been actively involved for more than 30 years in charitable and volunteer service (Red Cross, Tsunami Relief, and Blind Community) for public causes.

Notes

[1]F. E. Terman , *Radio Engineers Handbook*, pp. 498 ff, McGraw-Hill Inc, NY, 1943, ASIN: B000GWIWFM.

[2]F. Langford-Smith, Editor, *Radiotron Designers Handbook*, pp. 947 ff., Electron Tube Div. RCA, Harrison, NJ, 1954, ASIN: B000JILVH4.

[3]L. J. Giacoletto, *Electronics Designers Handbook*, p. 16-1, McGraw Hill Book Company, Inc, NY, 1977.

[4]F. Vilbig, *Lehrbuch der Hochfrequenztechnik*, Vol. 2, pp. 235, Akademische Verlagsgesellschaft Becker & Erler Kom.-Ges., 1937/1942, ISBN: 9780070231498.

[5]K. L. Kotzebue and W. J. Parrish, "The use of large signal S-Parameters in microwave oscillator design," in *Proc. 1975 Int. Microwave Symp. On Circuits and Systems*.

[6]V. Rizzoli, A. Neri, A. Costanzo, F. Mastri, "Modern Harmonic-Balance Techniques for Oscillator Analysis and Optimization," in *RF and Microwave Oscillator Design*, ed. M. Odyniec, Artech House, 2002.

[7]W. Anzill, F.X. Kaertner, P. Russer, "Simulation of the Single-Sideband Phase Noise of Oscillators," *Second International Workshop of Integrated Nonlinear Microwave and Millimeterwave Circuits*, 1992.

[8]G. Gonzalez, *Foundations of Oscillator Circuit Design*, Artech House, Inc., 2007, ISBN 10: 1-5963-162-0.

[9]U. L. Rohde, A. K. Poddar, and G. Boeck, *The Design of Modern Microwave Oscillator for Wireless Applications Theory and Optimization*, ISBN 0-471-72342-8.

[10]K. M. Johnson, "Large Signal GaAs MESFET Oscillator Design", *IEEE Trans. on MTT-27*, No. 3, Mar 1979.

[11]K. K. Clarke, "Design of Self-Limiting Transistor Sine-Wave Oscillator", *IEEE Transaction on Circuit and Systems*, [legacy, pre-1988], vol. 13, Issue 1, Mar 1966, pp. 58-63.

[12]U. L. Rohde and J. Whitaker, *Communication Receivers: DSP, Software Radios, and Design, Third Edition*, McGraw-Hill, pp.413-422, 2001, ISBN:0-07-136121-9.

[13]U. L. Rohde and D. P. Newkirk, *RF/Microwave Circuit Design For Wireless Applications, 2000*, pp.798-812, 413- 422, ISBN:0-471-29818-2.

[14]M. Gitterman, *The Noisy Oscillator The First Hundred Years, From Einstein Until Now*, World Scientific Publishing Co., 2005, ISBN 981-256-512-4.

[15]M. Tiebout, *Low Power VCO Design in CMOS, Springer Series in Advanced Microelectronics*, Springer Berlin Heidelberg 2006, World Scientific, Singapore 596224, 2005, ISBN: 3-540-24324-0.

[16]E. Camargo, *Design of FET Frequency Multipliers and Harmonic Oscillators*, Artech House, Inc, 1998, ISBN 0-89006-481-4.

[17]R.I W. Rhea, *Oscillator Design And Computer Simulation, Second Edition*, SciTech Publishing, 911 Paverstone Dr., Raleigh, NV 27615, 2006, ISBN: 1-884932-30-4.

[18]M. Odyniec, Editor, *RF And Microwave Oscillator Design*, Artech House, Inc., 2002, ISBN 1-58053-320-5.

[19]Peter Vizmuller, *RF Design Guide: Systems, Circuits and Equations*, Artech House, 1995, ISBN 0-890006-754-6.

[20]U. L. Rohde and A. K. Poddar, "Impact of Device Scaling on Oscillator/VCO Phase Noise in SiGe HBTs," *International Semiconductor Device Research Symposium*, ISDRS 2005, USA, December 7-9, 2005.

[21]U. L. Rohde and A. K. Poddar, "Reconfigurable Concurrent Oscillators For Multi-Band Multi-Mode Wireless Communication Systems", *IEEE Sarnoff Symposium*, Princeton, NJ, 30 April - 02 May 2007.

[22]U. L. Rohde and A. K. Poddar," Wideband voltage controlled oscillators employing evanescent mode coupled resonators," *US Patent* 7,180,381, Feb 2, 2007.

[23]U. L. Rohde, A. K. Poddar, and R. Rebel," Integrated Low Noise Microwave Wideband Push- Push VCO", *US Patent* 7,088,189, Aug 2006.

[24]D. B. Leeson, "A Simple Model of Feedback Oscillator Noise Spectrum", *Proceedings of the IEEE*, Feb. 1966, 54 (2), pp. 329–330.

[25]**www.microwavejournal.com/articles/29151-noise-analysis-then-and-today?v=preview**.

[26]Ulrich L. Rohde and Anisha M. Apte, "Everything You Always Wanted to Know About Colpitts Oscillators", *IEEE Microwave Magazine*, Aug. 2016, pp. 59-76.

Matthew H. Reilly, KB1VC

10312 Breconshire Road, Ellicott City, MD 21042; **kb1vc@kb1vc.org**

The Arduino: An Electronic Tinkertoy

The Arduino ecosystem includes a wide variety of easy-to-use integrated hardware components, and software development environment.

A version of this article appeared in *The Proceedings of the 2016 VHF Super Conference*, April 15 and 16, 2016.

Formerly, no matter which micro-controller or small processor one chose, the challenge of building a software environment, acquiring parts, digging through documentation, and navigating errata often took so much effort that it was easy to forget why a micro-controller seemed like a good idea at the start. The Arduino development environment allows any ham to use a micro-controller to sequence relays, drive odd interfaces, monitor widgets remotely, or even build impromptu one-off test equipment. Often there is no need to create a special module, as many interesting input-output options are available off the shelf, thanks to the maker culture.

This article aims to introduce the Arduino hardware and software components. It is not a how-to guide, but aims to provide a starting point for newcomers to the Arduino environment.

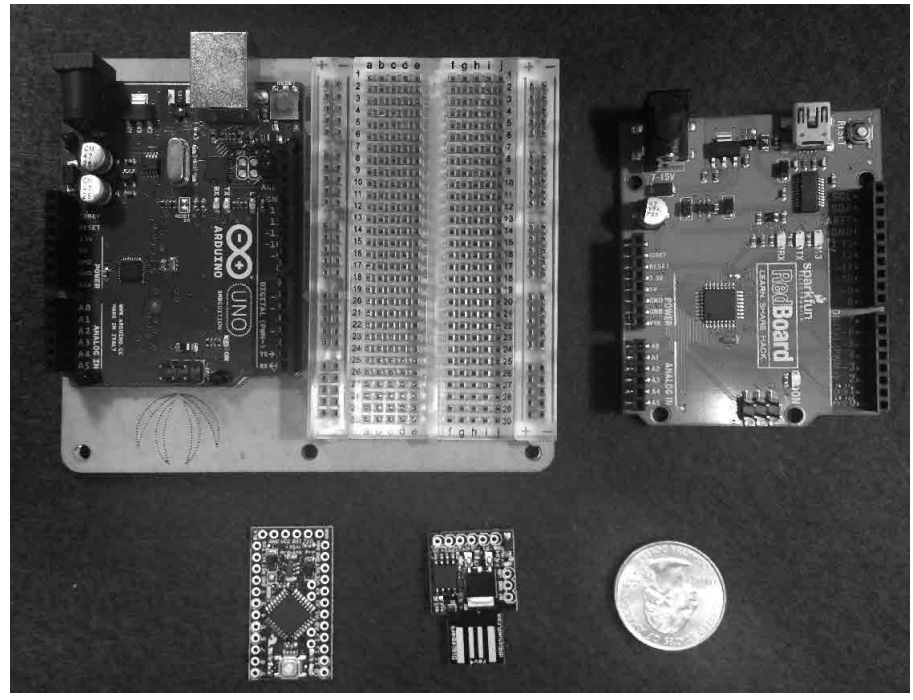

Figure 1 — Four Arduino processor modules: clockwise from upper left – UNO with protoboard, SparkFun RedBoard, US quarter-dollar coin (24.26 mm diameter), Digispark, and Arduino Pro Mini.

1 — Just What Is an Arduino?

Arduino is a company. It is a user community. It is an open-source hardware architecture (of sorts). It is a development environment. It is a set of libraries. Arduino is a viable solution for many Amateur Radio related embedded computing applications. If you need a programmable widget to sequence a set of operations, control a servo, actuate a relay, or monitor a process, an Arduino solution may well be in your future.

Arduino started out as a student project in 2005 at the Interaction Design Institute in Ivrea, Italy. Wikipedia tells the whole story (**https://en.wikipedia.org/wiki/Arduino**).

Most Arduino processor modules are built around one of the many Atmel 8, 16, or 32 bit AVR micro-controller chips. But new modules using the ARM instruction set are being introduced every day. All of them share the same programming model, tool chain kit, and many of the libraries. That's what makes Arduino an attractive platform for quick projects and simple controllers. The Arduino integrated development environment even supports the x86-based Intel Edison embedded computing platforms. This introduction will concentrate on the AVR series, as most of the Arduino world revolves around the simpler architecture of the Atmel chips.

The key point here is that Arduino

means a lot of different things. But the most important attributes of the Arduino ecosystem are the wide availability and variety of hardware components, and the extremely easy-to-use integrated software development environment.

2 — Arduino Hardware

2.1 — Processors

Considering only the Atmel/AVR Arduino widgets, there are more than a dozen choices. I've settled on the four shown in Figure 1.

Arduino Uno R3 — This is as close as Arduino comes to a standard module. It has two rows of connectors — one on each side — that mate with any standard Arduino shield. Many vendors offer this board. The Uno provides 14 digital I/O pins, 6 analog inputs that share a common 10 bit A/D converter, 6 PWM outputs that share physical pins with 6 of the digital I/Os, and a UART. The typical price for a model from SparkFun or Adafruit is around US$25.

SparkFun RedBoard — This is nearly identical to the Arduino UNO, but manufactured by SparkFun. The difference with respect to the Uno R3 is in a subtle and irrelevant-to-the-user choice in the part that does the USB to UART conversion. The RedBoard is available from SparkFun for $20.

Arduino Pro Mini 5V — This module is not physically compatible with typical shields. It is, however, cheaper and physically half the size of the UNO/RedBoard. It uses the same processor and has the same complement of I/O pins (plus two additional analog inputs) as the full size modules. It does not provide a USB interface. The programming path and any serial I/O must be via a separate FTDI module. The Pro Mini is available from a number of vendors for about US$10. The FTDI serial converter is available from SparkFun for US$15.

Digispark — This is a very small module with just 6 I/O pins. Four can be used for digital I/O or analog input to a shared ADC. Three pins support timer-based PWM. The module plugs directly into a USB host socket for programming. Digispark modules are available from **www.digistump.com** for US$9 each.

For quick proof-of-concept experiments or for throw-away tests, I'll use an UNO that sits on the workbench and is glued to a plate that holds a small 30-row prototype poke board. It was the first Arduino that I bought, and is a fixture in the shop.

For prototypes and other projects where the task can be accomplished with off-the-shelf shields, I use a RedBoard. A Jack-o-Lantern project, and several of the robots that my son and I have built used the RedBoard.

The T/R switch in my 10 GHz transverter is built around a Digispark, as it was small and fit in the box that held the four relays and the opto-isolator.

For projects that warrant a special PC board, the Pro Mini is the obvious choice. It is inexpensive, sturdy, and small. I've used it most recently in a line-follower robot and in the serial-controlled T/R and band switch for a software defined radio.

2.2 — Shields

An embedded processor without I/O widgets is useful only as a heat source, and a feeble one at that. The Arduino community has produced a huge variety of I/O units that plug into a standard pin footprint on the Arduino UNO and its many clones. Not all Arduino processors can connect directly with a shield — remember Arduino is as much about the programming environment as the actual hardware widget. But all the shields are compatible with the UNO or RedBoard that were described earlier.

Figure 2 shows four typical shields. There are dozens more. SparkFun alone lists more than 30 different shields in their catalog. Among them:

- an XBee transceiver
- a CAN-BUS interface
- a weather sensor interface
- an MP3 player
- an H-bridge driver for two dc motors
- a MIDI interface
- a capacitive touch sensor array.

Shields can often be stacked, provided that two shields don't use the same I/O pin for incompatible purposes. Figure 3 shows a stack of two shields on a RedBoard. The middle shield started out life as a blank array of plated-through vias. These were used to host a DDS module that required just a few Arduino I/O pins for control.

3 — Arduino Software

The key distinction between an Arduino solution and one built on a general purpose PC or even a simple platform like a Raspberry Pi is the absence of an operating system. In fact, it is possible to build an Arduino application where the programmer can see every single line of code involved in executing the program, including the I/O operations. This would be a spectacular disadvantage in developing fancy GUI applications or large data processing programs, or even a complete software defined radio. But in the case of an embedded computing application, like sequencing the transmit/receive switching in a transverter, simplicity is the key to ensuring

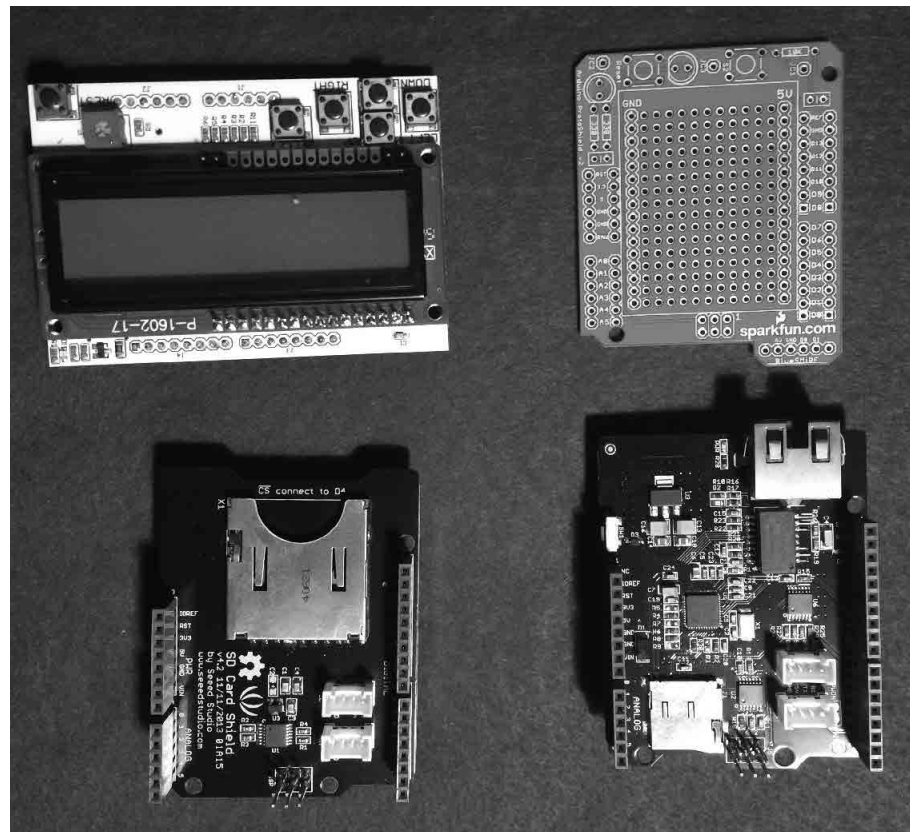

Figure 2 — Four Arduino shields: clockwise from upper left – 20x2 LCD display with buttons, prototype shield, Ethernet shield, SD card shield.

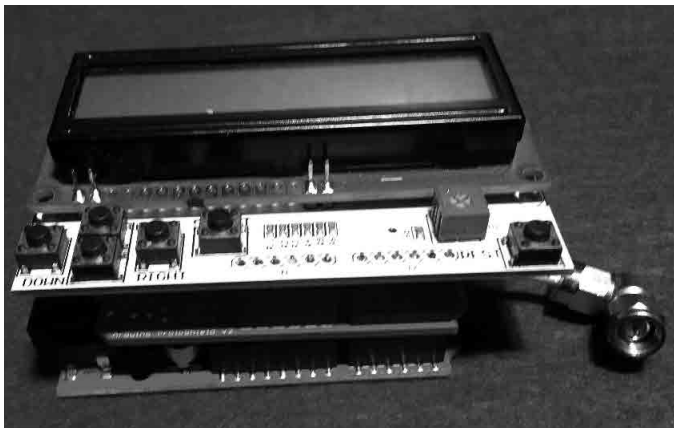

Figure 3 — A 40 MHz frequency generator in two shields: RedBoard (bottom), proto shield with DDS unit (middle), and 20x2 LCD display (top).

Figure 4 — Arduino sketch to toggle a relay coil on and off at 2 second intervals.

that our computer-based solution is more reliable than the analog-based design that it replaces. Where we might use an Arduino to build an impromptu lab instrument — like the relay experiment described later in this paper — the simplicity of the software stack ensures that we spend our time understanding our experiment, rather than debugging our test instrument.

3.1 — The Arduino IDE

All real embedded computing widgets — PIC, BasicStamp, Arduino, Edison — sport some kind of integrated development environment (IDE). The Arduino IDE is built around the notion of a "sketch." A sketch is a C++ program, contained in a single file, that describes the initialization of an Arduino, and at least one action routine. C programmers who are leery of C++ as an embedded controller language need not worry. This is not esoteric C++. The C++ aspects are truly a convenience and don't appear to cause performance, readability, or maintainability problems. The initialization routine (setup()) is called right after RESET is de-asserted, and must setup all internal registers and any static state for the sketch. There may be many other routines defined in the sketch, but exactly one of them must be named loop(). The loop routine is called by the Arduino run-time supervisor. The supervisor itself is an infinite loop containing a call to loop() and a call to a routine to maintain a wall-clock time counter.

Figure 4 shows an Arduino sketch that toggles a relay on and off at 2 second intervals. There's not much to it. The setup routine initializes the I/O pin control registers to handle pin 2 as a digital output. The loop routine turns the relay on or off, then sleeps for 2 seconds before returning to the run-time supervisor. Then it gets called again, and again, and so on.

The menu bar at the top of Figure 4 as the typical File and Edit pull-down menus. In addition the Sketch pulldown provides options to compile the sketch, download it into a module, and import various support libraries. Most shields come with associated support libraries so that sketch writers need not be concerned with subtle details of the hardware, like which register turns on the backlight, or how to write a block of data to an SD card. The Tools pulldown allows the programmer to identify the target Arduino module type. There are dozens of different hardware modules that are compatible with the Arduino IDE. Within the Atmel/AVR family, they range from units like the Digispark, with a simple 16.1 MHz CPU and just six I/O pins to the giant Arduino Mega 2560 with 54 I/O pins, and 256 kB of flash memory. All can be programmed from the same IDE and many sketches require no changes at all to run on any module type.

3.2 — Libraries

The Arduino community includes many tinkerers, students, geeks, and folks who stay up late at night. They are prolific and eclectic. Chances are, if a device can be controlled with a few digital I/O lines, there's an Arduino application that uses it. And if the device gets used by more than one person, it has a library to support it. The Arduino IDE comes with dozens of software libraries that provide C++ classes to encapsulate the functions of the device. For instance, many Arduino applications need to communicate with a PC host via a USB link.

Example 1.
"Hello World" in the Arduino IDE.

```
void setup() {
  Serial.begin(9600);
}
void loop() {
  Serial.println("Hello World!");
}
```

Some Arduinos implement a TTY serial link over USB, while others rely on an external FTDI USB to RS232 interface. The Arduino IDE comes with a serial library that hides all that complexity. For example, the *Hello World* program for Arduino UNO is in the Example 1. The setup routine initializes the serial port for 9600 baud. The loop routine prints "Hello World" followed by a carriage return until the Arduino is disconnected from the USB cable.

The ease of use and wide community support comes at a price however. The

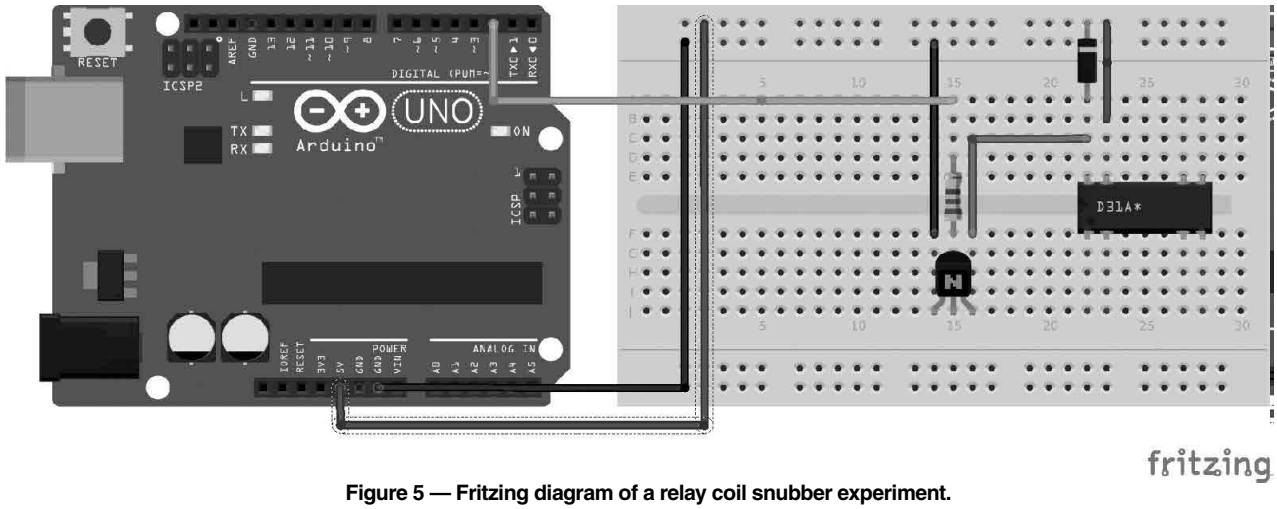

Figure 5 — Fritzing diagram of a relay coil snubber experiment.

Arduino ecosystem is built largely on the work of volunteers and students. Like folk music, some of it is quite good, and some of it is "written by folk." Nevertheless, a typical Arduino project can show "good enough" results with just a few hours or even minutes of work, and then provide infinite opportunities for improvement or elaboration.

4 — Arduino as a Lab Instrument

In the past three years, I've used Arduinos to build a T/R sequencer for a 10 GHz transverter, a T/R and bandswitch for a 10 MHz to 6 GHz software defined radio, four battle bots, two line-follower robots, and a Jack-o-Lantern that makes rude noises when its IR motion sensors are triggered. But I've also used Arduinos as impromptu lab instrument controllers. One excited the coil of a 5 V relay to demonstrate the importance and effectiveness of snubber diodes across inductive loads. A second monitored the temperature of a noise source. This section describes these two simple instruments.

4.1 — Are Snubbers Important?

Now and then we all forget the fundamentals, or encounter a colleague who has done the same. Often a quick and low-risk experiment can bring us back to reality. The Arduino provides a convenient and cheap sandbox for simple experiments.

For instance, how important are snubber diodes across low power relay coils? Figure 5 shows a simple Arduino configuration that drives a relay coil via the junk box favorite 2N4124. This drawing was produced with the "Fritzing" documentation and design program, **www.fritzing.org**. The snubber diode, a 1N645 across the coil, will clamp the low end of the relay coil to a bit over 8.5 V before settling to about 6 V in about 200 nS.

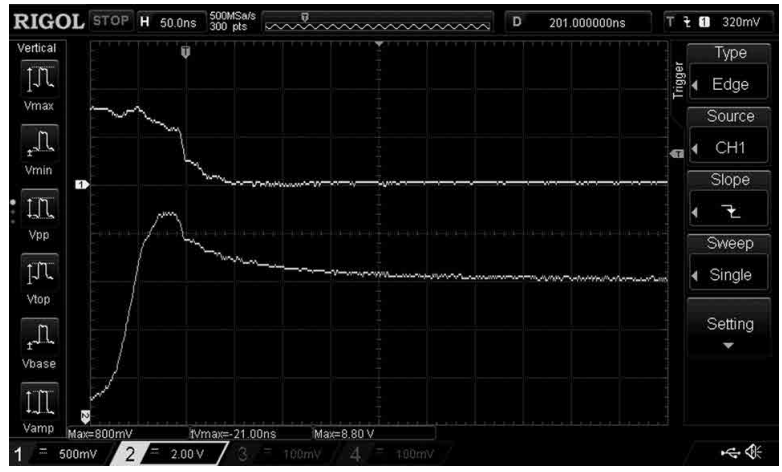

Figure 6A — Driver collector voltage with snubber diode. Upper trace shows the voltage at the base of the transistor. The lower trace is the voltage at the collector and the lower end of the relay coil.

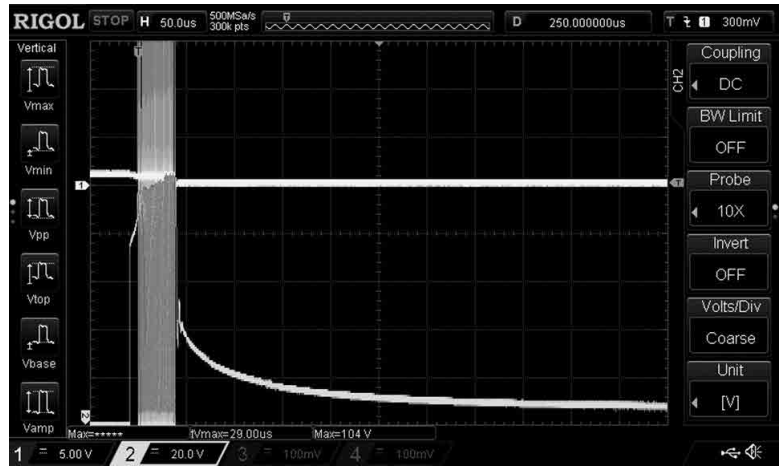

Figure 6B — Driver collector voltage without snubber diode. Upper trace shows the voltage at the base of the transistor. The lower trace is the voltage at the collector and the lower end of the relay coil.

Figure 7 — Thermal sensors and noise source in frozen linseed oil.

Example 2

Temperature monitor sketch for Arduino and DS18B20 sensors.

```
#include <OneWire.h>
#include <DallasTemperature.h>
/* Code inspired by
 * http://www.hobbytronics.co.uk/ds18b20-arduino
 * OneWire library from
 * https://github.com/PaulStoffregen/OneWire
 * Dallas sensor library from
 * https://github.com/milesburton/Arduino-Temperature-Control-Library
 */
#define DS18B20_IN 2
OneWire bus(DS18B20_IN);
DallasTemperature sensors(&bus);
void setup() {
  Serial.begin(9600);
  sensors.begin();
}
void loop() {
  int i;
  sensors.requestTemperatures();
  for(i = 0; i < 2; i++) {
    float temp = sensors.getTempCByIndex(i);
    Serial.print(temp + 273.15); Serial.print(" ");
  }
  Serial.println();
  delay(1000);
}
```

We saw the code to control the relay back in Figure 4. It is designed to flip the relay at 2 second intervals to allow the 2N4124 to recover from the abuse it receives on each falling edge of V_{be}.

The upper trace in Figure 6A shows the voltage at the base of the transistor. The lower trace is the voltage at the collector and the lower end of the relay coil. Figure 6B shows the same terminals with the 1N645 snubber removed from the circuit; note the very different scales relative to Figure 6A. The 2N4124 was not designed for the beating it is taking in the lower trace. Its maximum V_{ceo} rating is just 25 V, and we see spikes in the lower trace in excess of 100 V. This is well above what we'd expect for the collector-base breakdown voltage — specified as 30 V, minimum. This device appears to have held out to about 80 V before it succumbed.

Snubbers are important, my Arduino told me so. The scope pictures are from a Rigol DS1054Z oscilloscope.

4.2 — A Temperature Monitor

A few years ago, I wanted to see if the change in noise from a 50 Ω termination was detectable by an Ettus B210 software defined radio as the temperature was varied. The ultimate goal was to find a way to calibrate a home-built noise-diode noise source against a thermal noise source with "normal" household objects. This is what I had to work with:

1 — A collection of SMA attenuators up to 20 dB and covering 50 MHz to a few GHz.

2 — An aluminum block about 1 x 2 x 4 inches

3 — A few DS18B20 one-wire digital temperature sensors (range -55 to +125 °C)

4 — Arduino UNO

5 — A drill press

6 — A source of dry ice

7 — A quart of linseed oil

8 — An Ettus USRP B210 software defined radio.

When a material passes from its liquid state to its solid state, the mass of the material tends to stay at the freezing point, even while part of the block is solid and the rest is a slurry. For this experiment, I inserted the thermal sensors and the actual device under test into a tub of oil, and slowly cooled it to its freezing point. At the freezing point, the sensor and device arrived at the freezing point of the oil and stayed there long enough to do many measurements.

The web told me that linseed oil would freeze at about -50 °C. It must be true, it is on the web. So I drilled holes in the aluminum block that were a press fit for the sensor packages and a 20 dB attenuator. I pressed the attenuator and a 50 Ω termination into the center hole, and the sensors in two holes on either side of the termination. The attenuator was connected to the RF input of the Universal Software Radio Peripheral (USRP), and the temperature sensors were connected to two A/D inputs on the Arduino.

The block of aluminum was immersed in a tub of linseed oil. The tub was surrounded by blocks of dry ice. The whole mass of dry ice and oil was placed in a cooler. Within a short time, the linseed oil had frozen. Alas, linseed oil that we buy at the hardware store today has additives that change its freezing point. The block got down to about 233K (-40 °C). Figure 7 shows the frozen block of linseed oil surrounded by dry ice with the thermal noise source submerged in the frozen bath.

It took several hours for the block of oil to thaw. In the mean time, a program running on a Linux workstation monitored the temperature measurements from the Arduino and measured the magnitude of the noise signal coming from the I/Q ports of the SDR. The thermal mass of the aluminum block and the blob of linseed oil was such that the temperature of the noise source changed very slowly.

The code to run the software defined radio was quite complex, but the Arduino sketch to measure and report the temperature was so simple, I didn't even save it. I recently recreated this code using the time-honored programming technique called "copying stuff from other people." The Fritzing drawing of the configuration is shown in Figure 8, and the code is shown in Example 2.

The Arduino program uses two libraries that were downloaded from GitHub. This is

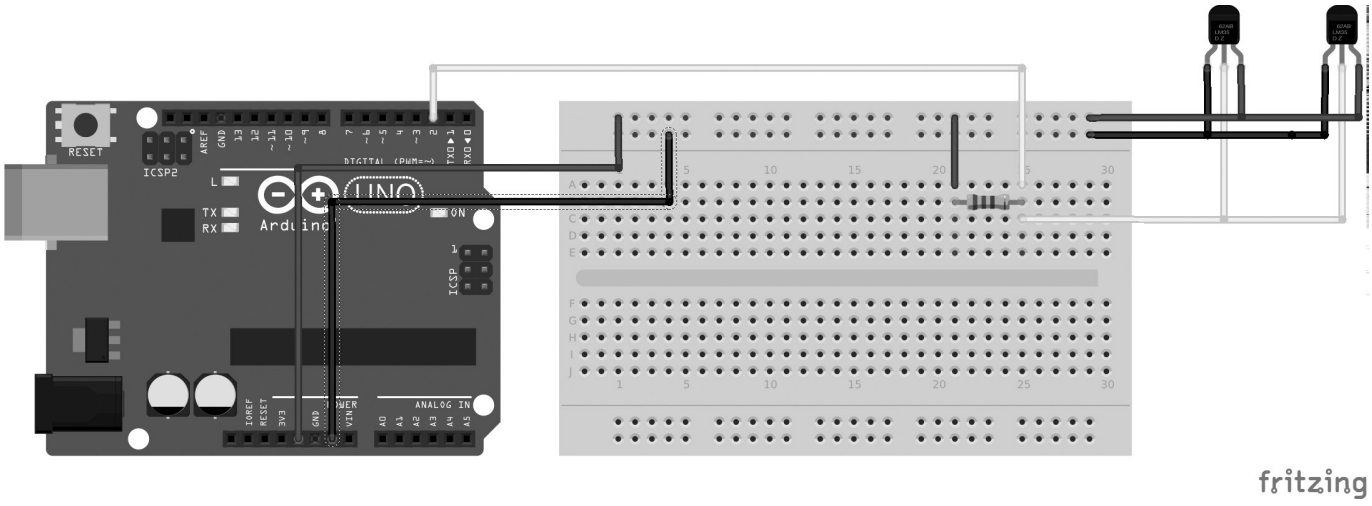

Figure 8 — Fritzing diagram of Arduino UNO and two thermal sensors.

a general theme in the Arduino community. If you don't find what you want in the basic Arduino development kit, a solution is likely out there that will get you through the next step. In this case, the thermal sensors were Dallas Semiconductor devices that use the OneWire communication protocol. A few online searches produced the necessary libraries.

Figure 9 shows the relative noise power at two selected frequencies, one in the 2 m band (upper trace) and the other in the 2304 MHz band (lower trace). With time and refinement, measurement like this might lead to a method of rough calibration for home-built noise sources.

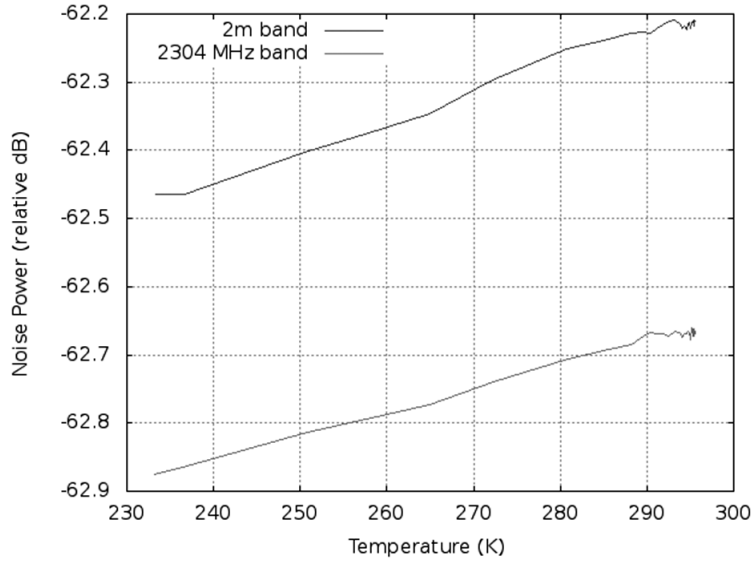

Figure 9 — Relative noise power vs. terminator temperature may lead to a method of rough calibration for home built noise sources. The upper curve is for the 2 m band, and the lower curve is for 2304 MHz band.

5 — Conclusion

The Arduino development environment is easy to use and has all that you could need to build simple controllers, manipulators, and other one-off widgets. It is all available on the web. A good starting place is **www.arduino.org**.

Numerous vendors offer scores of options for Arduino compatible processors and I/O devices. SparkFun (**www.sparkfun.com**) and Adafruit (**www.adafruit.com**) offer many components and modules that are affordable and convenient.

With a strong software tool set, and a huge variety of off-the-shelf components, Arduino is my first choice when I consider building a sequencer, robotic device, or quick-and-dirty laboratory instrument. Its simplicity, specifically the absence of an elaborate operating system, simplifies the task of coding real-time applications. Its huge variety of components, ranging from the pedestrian (stepper motor drivers) to the truly odd (sixteen channel model airplane servo drivers) allow for fast prototype development, and often instant proof-of-concept models.

Matt Reilly, KB1VC, was first licensed in 1979. He graduated from Virginia Tech with a BSEE in 1981 and from Carnegie Mellon University with a PhD in Computer Engineering in 1989. While a computer engineer by trade, he is a radio geek by avocation. For the past five years Matt has been developing SoDaRadio, an all-mode software defined radio, and various Arduino based widgets ranging from transmit/receive switches to toy battle-bots. Matt lives in Maryland with his wife and young son.

A Better RF Voltmeter Probe

An RF voltmeter probe connected to a DMM or VTVM is used by many experimenters. The probe consists of a diode, capacitor, and one or more resistors enclosed in a housing with a contact tip on one end. Suitable leads connect the probe output to a high-input-impedance, dc-reading meter.

In many applications, the probe's relative response is all that is needed, and the above-described setup is sufficient. There are times, however, when the actual RF input peak voltage is of interest. For a sufficiently high peak-voltage input, this quantity is approximated by the DMM reading. Otherwise, for low-voltage inputs, the DMM displays a dc voltage reading that is approximately proportional to the diode square-law response. In what follows, a technique is described that may lead to more accurate peak-voltage measurements over much larger ranges of input RF voltage.

Circuit and Basic Assumptions

Consider the RF probe depicted by Figure 1. Assumptions can be made to simplify the analysis of this circuit. Assume that the probe does not significantly "load" the circuit node under test, a condition that holds if $|Z_s|$ is sufficiently small. That is, assume that the quantity $A\sin(\omega t)$ is the approximate voltage at the probe tip, and $v_D \approx \alpha_0 + A\sin(\omega t)$ is across the diode, where α_0 is a positive dc voltage slightly smaller than A. This assumption is reasonable given that the diode is forward biased over a small fraction of each RF cycle, only at the negative-most extremes of the input sinusoid. Components R_3 and C_2 are selected to keep RF out of the CA3260A MOSFET-input op-amp (with a typical dc input resistance on the order of 10^{12} Ω). Finally, diode current i_D in Figure 1 is approximated by the Schottky equation,

$$i_D \approx I_S\left[\exp\left\{\frac{-(\alpha_0 + A\sin(\omega t))}{\eta V_t}\right\} - 1\right]$$

where I_S denotes the reverse-saturation current, η is the diode ideality factor, and V_t is the thermal voltage,

$$V_t \approx 8.617\times10^{-5}(T + 273.15)\ .$$

The diode junction capacitance C_{j0} is less than 1 pF for a BAT68. It is neglected here, an assumption that is valid for frequencies in the HF range, if not somewhat higher.

AC Voltmeter Equation

Sum the currents that enter the junction of D_1 and R_1. This sum must have a zero dc component, a constraint that ultimately leads to

$$\exp\left[\frac{-\alpha_0}{\eta V_t}\right]\underbrace{\frac{1}{2\pi}\int_0^{2\pi}\exp\left[-\frac{A}{\eta V_t}\sin(x)\right]dx}_{I_0\left(\frac{A}{\eta V_t}\right)} - 1 = \frac{\alpha_0}{I_S R_1} \qquad (1)$$

where $I_0(x)$ is the zero-th order modified Bessel function. Hence, the reformulated constraint Eq 1. simplifies to

$$\exp\left[\frac{-\alpha_0}{\eta V_t}\right] I_0\left(\frac{A}{\eta V_t}\right) - 1 = \frac{\alpha_0}{I_S R_1} \qquad (2)$$

The op-amp compensation circuit is used to eliminate the reverse-saturation current I_S from the final results. This is important since I_S is highly temperature dependent, approximately doubling for every 5 °C increase in temperature. To obtain the elimination of I_S, note that op-amp operation can be described by

$$\exp\left\{\frac{(\alpha_1 - \alpha_0)}{\eta V_t}\right\} - 1 = \left(\frac{R_1}{R_2}\right)\frac{\alpha_0}{I_S R_1} \qquad (3)$$

Now, substitute Eq 2 into Eq 3 and obtain

$$\exp\left\{\frac{(\alpha_1 - \alpha_0)}{\eta V_t}\right\} - 1 = \left(\frac{R_1}{R_2}\right)\left[\exp\left(\frac{-\alpha_0}{\eta V_t}\right) I_0\left(\frac{A}{\eta V_t}\right) - 1\right] \qquad (4)$$

If $R_1 = R_2$, Eq 4 simplifies to the *ac voltmeter equation*

$$I_0\left(\frac{A}{\eta V_t}\right) = \exp\left\{\frac{\alpha_1}{\eta V_t}\right\} \qquad (5)$$

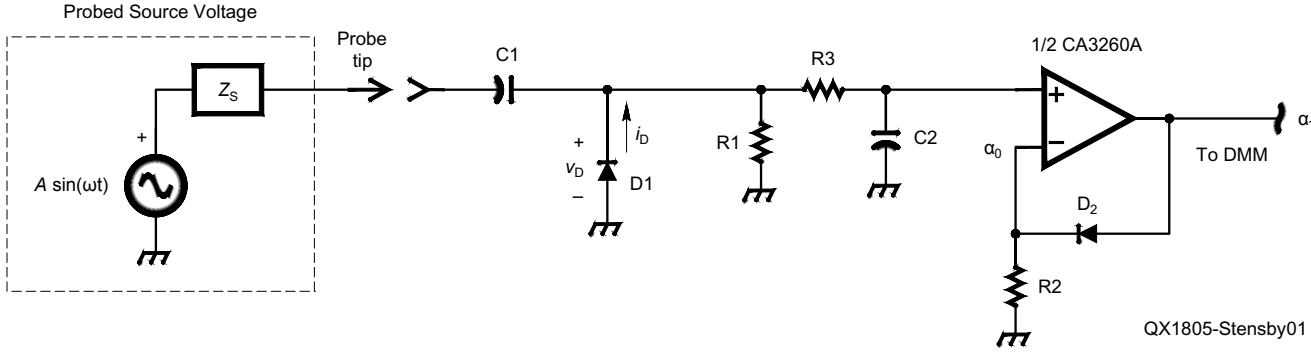

Figure 1 — An RF probe.
C1, C2 — 1000 pF mica chip capacitor
D1, D2 — Infineon BAT68
R1, R2 — 1 MΩ 1% metal film resistors
R3 — 10 MΩ 1% metal film resistors

a result that may be new to the literature. Note that temperature-dependent, reverse-saturation current I_S does not appear in Eq 5. Given a measured value for α_1, Eq 5 can be solved for the input peak voltage *A*.

Solution Technique and Numerical Results

In application, a DMM (or VTVM) is used to measure dc voltage α_1. Then, Eq 5 is solved numerically for *A*. There are many software packages, some of them free, which can accomplish this. For example, Table 1 lists a simple *GNU Octave* (or *Matlab*) command line script that can solve Eq 5 for *A* given inputs α_1, η and temperature *T* in degrees Celsius.

Normally, many experimenters use measured α_1 as an estimate of *A*, an approach that may lead to a significant error, as is suggested by Figure 2. For $0.1 \leq \alpha_1 \leq 4$ and two values of temperature (that bracket room temperature *T* = 26.85 °C by ±20%), Figure 2 depicts plots of percent error $100(A - \alpha_1)/A$, where *A* is the solution of Eq 5. As expected, the error increases significantly as α_1 approaches zero.

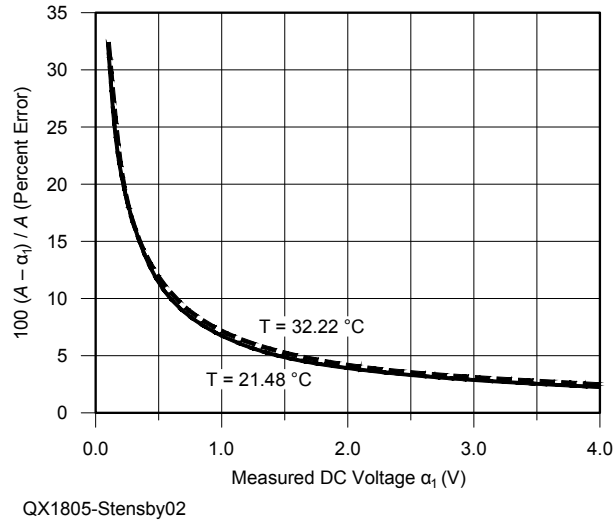

Figure 2 — Percentage difference between computed *A* and measured α_1.

Table 1.

Solve the ac voltmeter equation with this GNU Octave script.

```
% RFvoltmeter.m
a1 = input('a1 = ');
n = input('Ideality = ');
T = input('Temperature in Degrees Celsius = ') + 273.15;
% Boltzmann constant Kb = 8.617332478e-5 ev/degree-Kelvin
Vt = n*8.617332478e-5*T;
f = @(A) exp((a1-A)/Vt) - exp(-A/Vt)*besseli(0, A/Vt);
A = fsolve(f, a1)
```

An algorithm is provided here for improving the accuracy of simple diode-based ac/RF voltmeter probes. It can be programmed into microprocessor-based, low-cost instrumentation. It can be extended easily. Possible extensions include 1) incorporating the diode junction capacitance in the analysis, 2) including in the diode voltage model additional spectral components (i.e., harmonics), and 3) use of a thermometer-on-a-chip IC (such as the LM35) to provide accurate temperature data. — *Dr. John Stensby, N5DF,* ***stensbj@uah.edu***.

Send your short *QEX* Technical Note to the Editor, via e-mail to qex@arrl.org. We reserve the right to edit your Note for clarity, and to fit in the available page space. "*QEX* Technical Notes" may also appear in other ARRL media. The publishers of *QEX* assume no responsibilities for statements made by correspondents.

Letters

Design of a Two-band Loaded Dipole Antenna, (Sep/Oct 2017)

Dear Editor,

I was very impressed with the David Birnbaum, K2LYV, article. David's application of the method of Lopes to compute the reactances of two desired resonant frequencies in the two-band loaded dipole antenna is quite innovative. My admiration comes from my failed attempts to identify a procedure to solve this somewhat complex problem in the past. I modeled David's 30 / 20 meter design example in EZNEC and with a slight shortening of the dipole end wires, the SWR low points exactly matched David's results. This motivated me to repeat David's design steps for his example using the Lopes method, which in turn would validate this method for the design of other two-band dipoles. I had some difficulty in applying the Lopes method to exactly reproduce David's example, which as stated was verified with EZNEC. I chose to use an alternative method that avoids the Lopes calculations that might be of interest to others.

For this, I modeled two dipoles in EZNEC with the target 30 / 20 meter dipole length and trap locations. The first dipole used an inductor at the trap location. This inductor value was varied in an iterative manor to produce an SWR minimum for the lower resonant frequency of the target 30 / 20 meter trap dipole. The reactance of the inductor at this frequency is X_1 needed in David's calculations. The same process was used for the second dipole where a capacitor was placed at the trap location. The capacitor value was iteratively adjusted to produce an SWR minimum at the higher resonant frequency of the target 30 / 20 meter trap dipole, which in turn yielded X_2. These values for X_1 and X_2 were then used in David's calculations to identify the 30 / 20 meter dipole trap resonant frequency along with the trap L and C values. These values applied to an EZNEC simulation, again with a slight shortening of the dipole end wires, exactly matched the target low SWR points for the two desired frequencies. — *73, David Brown, K3CTN; dbbrown624@gmail.com.*

Upcoming Conferences

2018 Central States VHFS Society, Inc. Conference

Wichita, Kansas
July 26-29, 2018
www.2018.CSVHFS.org

Call for papers: Papers are being solicited for publishing in the Proceedings of the 2018 Central States VHF Conference on all weak-signal VHF and above Amateur Radio topics, including: antenna modeling, design, arrays, and control; test equipment: including homebrew, commercial, and measurement techniques and tips; construction of equipment such as transmitters, receivers, and transverters; operating, contesting, roving, and DXpeditions; RF power amps, single and multi-band vacuum tubes, solid-state, and TWTAs; propagation, ducting, sporadic E, tropospheric, meteor scatter; amplifiers (low noise); digital modes, such as WSJT-X, JT65, FT8, JT6M, ISCAT, etc.; regulatory topics; moon bounce (EME); software-defined radio (SDR); and digital signal processing (DSP).

Topics such as FM, repeaters, packet radio, etc., are generally considered outside of the scope of papers being sought. However, there are always exceptions. If you have any questions about the suitability of a particular topic, contact **wa2voi@mninter.net**.

You do not need to attend the conference nor present your paper to have it published in the Proceedings.

Deadline for receipt of papers for inclusion in the Proceedings is Tuesday, May 15, 2018. Complete information, including a style guide, can be found on the Central States VHF Society, Inc. website.

ARRL/TAPR Digital Communications Conference (37th)

Albuquerque, New Mexico
September 14-16, 2018
www.tapr.org

The 37th Annual ARRL and TAPR Digital Communications Conference will be held September 14-16, 2018. in Albuquerque, New Mexico, at the Sheraton Albuquerque Airport Hotel. Rocky Mountain Ham Radio will be hosting the event.

The ARRL and TAPR Digital Communications Conference is an international forum for radio amateurs to meet, publish their work, and present new ideas and techniques. Presenters and attendees will have the opportunity to exchange ideas and learn about recent hardware and software advances, theories, experimental results, and practical applications.

Hotel and registration information will be available soon. Please check the website.

Call for Papers: Technical papers are solicited for presentation at the ARRL and TAPR Digital Communications Conference and publication in the Conference Proceedings. Annual conference proceedings are published by the ARRL. Presentation at the conference is not required for publication. Submission of papers are due by July 31st, 2018 and should be submitted to: Maty Weinberg, ARRL, 225 Main St., Newington, CT 06111

Topics include, but are not limited to: Software Defined Radio (SDR), digital voice (D-Star, P25, WinDRM, FDMDV, DRMDV, G4GUO), digital satellite communications, Global Position System (GPS), precision timing, Automatic Packet Reporting System™ (APRS), short messaging (a mode of APRS), Digital Signal Processing (DSP), HF digital modes, Internet interoperability with Amateur Radio networks, spread spectrum, IEEE 802.11 and other Part 15 license-exempt systems adaptable for Amateur Radio, using TCP/IP networking over Amateur Radio, mesh and peer-to-peer wireless networking, emergency and Homeland Defense backup digital communications, using Linux in Amateur Radio, updates on AX.25 and other wireless networking protocols, and topics that advanced the Amateur Radio art.

Microwave Update 2018

Dayton, Ohio
October 11-14, 2018
www.microwaveupdate.org

Microwave Update (MUD) is an international conference dedicated to microwave equipment design, construction, and operation. It is focused on, but not limited to, amateur radio on the microwave bands.

The Midwest VHF-UHF Society (MVUS) is pleased to host this event. The Conference will be held at the Holiday Inn in Fairborn, Ohio.

See website; more details will be posted as they become available.

24th Annual Pacific Northwest VHF-UHF-Microwave Conference

Seaside, Oregon
Oct 12-13, 2018
www.pnwvhfs.org

Join other weak-signal VHF, UHF and Microwave operators for the 24th Annual PNW VHF Society Conference to be held at the Best Western Ocean View Resort, 414 North Prom, Seaside, OR. Conference registration is $50 before October 1, or $60 thereafter and at the door.

See website; more details will be posted as they become available.

Errata

In Jeff Crawford, KØZR, "High Power HF Band-Pass Filter Design", *QEX* Mar./Apr. 2018, the labels for the ordinates in Figures 2 and 10 should be "Performance, dB", and the captions should continue: Filter S11, dB, (solid), and S21, dB, (dashed). The caption of Figure 12 caption should be "Measured S21, dB, performance of the filter". The trace in Figure 13 is S11, dB, and is actually the negative of the return loss, RL, (an error in the software package). The Figure 13 caption should be "Measured S11, dB, of the filter". We regret the error.

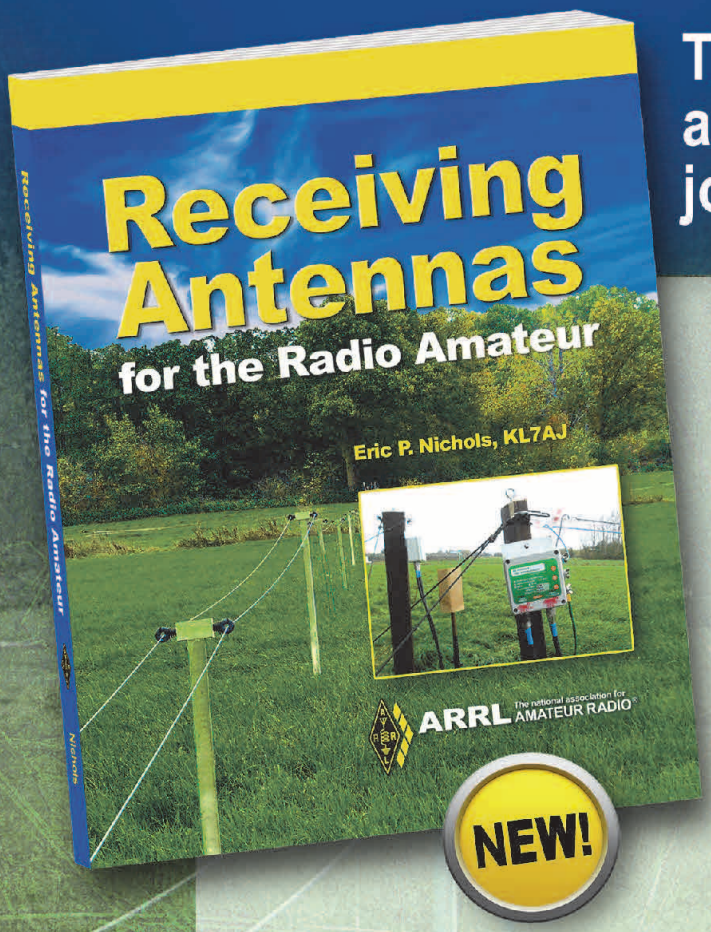

Transmitting and receiving antennas have different jobs to do.

Receiving Antennas
for the Radio Amateur

Eric P. Nichols, KL7AJ

Although the fundamental characteristics of antennas apply to both transmission and reception, the requirements and priorities of receiving antennas can be vastly different from those of transmitting antennas. ***Receiving Antennas for the Radio Amateur*** focuses entirely on active and passive receiving antennas and their associated circuits. There are relatively few cases where a radio amateur cannot benefit from a separate, well-designed receiving antenna or antenna system. On the low bands, including our new allocations at 630 and 2200 meters, heavy emphasis on the receiving end of these radio paths is essential for success.

The *active* antenna holds a prominent position in this book, as it offers good receiving performance while taking up minimal space. Recent developments in radio frequency (RF) semiconductors, especially low-noise RF operational amplifiers, have made a number of previously difficult-to-implement active antenna designs simple to build.

Table of Contents

Receiving Antennas For the Radio Amateur
ARRL Item No. 0789
ARRL Member Price! Only $24.95 (retail $27.95)

ARRL The national association for AMATEUR RADIO®

www.arrl.org/shop

Toll-Free US 888-277-5289,
or elsewhere +1-860-594-0355

QEX 5/2018

THE LATEST FROM STEPPIR:

new website!

STREAMLINED SHOPPING • LATEST NEWS • COMMUNITY • TECH INFO
PHOTOS AROUND THE WORLD • WORLD-CLASS STEPPIR SUPPORT

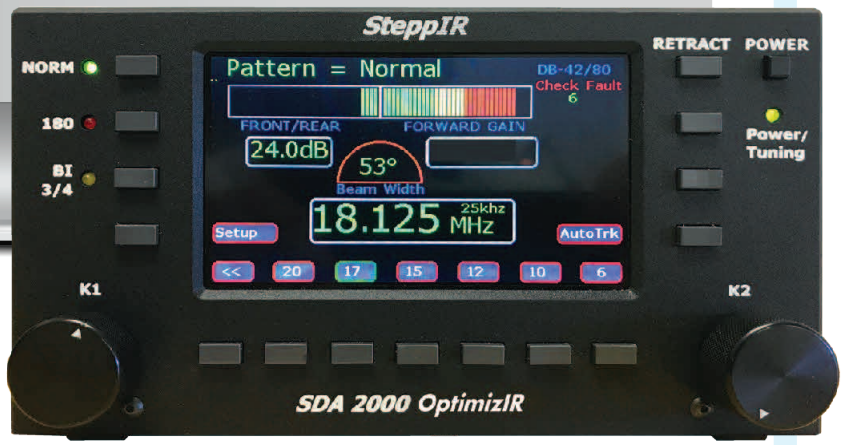

IT'S NOT A CONTROLLER, IT'S THE NEW STEPPIR SDA 2000

OptimizIR

CHECK IT OUT ONLINE!

steppIR
COMMUNICATION SYSTEMS

DETAILS & ORDERING:
www.steppir.com

Pre-Order

OptimizIR will be shipping first quarter 2018, accepting pre-orders now!

www.steppir.com
425-453-1910